LBL-10911

Lawrence Berkeley Laboratory
UNIVERSITY OF CALIFORNIA

Presented at the Nobel Symposium on High-Spin States, Orenas, Sweden, June 22-25, 1980; and submitted to Physica Scripta

THE DYNAMICS OF NUCLEAR COALESCENCE OR RESEPARATION

W. J. Swiatecki

June 1980

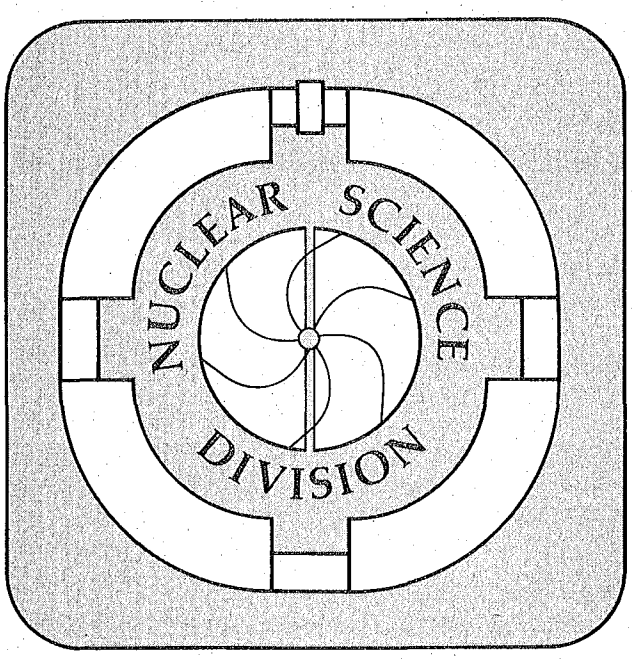

Prepared for the U.S. Department of Energy under Contract W-7405-ENG-48

DISCLAIMER

LBL-10911

THE DYNAMICS OF NUCLEAR COALESCENCE OR RESEPARATION

W. J. Swiatecki

Nuclear Science Division
Lawrence Berkeley Laboratory
University of California
Berkeley, California 94720

June 1980

Abstract

The dynamics of nuclear coalescence or reseparation. W. J. Swiatecki (Nuclear Science Division, Lawrence Berkeley Laboratory, Berkeley, CA).

A qualitative theory of the macroscopic dynamics of nucleus-nucleus collisions is presented. Attention is focused on three degrees of freedom: asymmetry, fragment separation, and neck size. The physical ingredients are a macroscopic (liquid-drop) potential energy [1], a macroscopic dissipation (in the form of the Wall- and Wall-plus-Window formulae [2,3]) and a simplified treatment of the inertial force. These ingredients are distilled into algebraic equations of motion that can often be solved in closed form. The applications include the calculation of the normal modes of motion around the saddle-point shapes, and the division of nuclear reactions into: a) dinucleus (deep-inelastic) reactions, b) mononucleus or composite nucleus (quasi-fission) reactions, and c) compound-nucleus reactions. Static and dynamic scaling rules are deduced for comparing different dinuclear reactions in a systematic way. Estimates are given for the critical curve in the space of target and projectile mass above which deep-inelastic reactions ought to make their appearance. The extra push over the interaction barrier needed to make two nuclei form a composite nucleus or else to fuse into a compound nucleus is also estimated.

I. Introduction

I would like to present a qualitative macroscopic study of what happens when two idealized nuclei touch, the neck between them grows, the mass

asymmetry begins to change and, eventually, either a compound nucleus is formed or the system reseparates. The stress will be on the greatest possible simplicity: I will focus on what I believe are a few of the essential physical ingredients of the process and I will then codify them into algebraic equations whose exploitation involves — in the main — only elementary functions and the solution of quadratic or, at most, cubic equations.

2. The dynamical ingredients

A dynamical theory often involves three types of forces: conservative, dissipative, and inertial. In this study, I will focus on the *macroscopic* aspects of the problem and will consequently use a macroscopic Potential Energy [1], and a macroscopic One-Body Dissipation Function [2,3]. As regards the inertial terms, I will make the following approximation: for necked-in shapes, when the communication between the two pieces is impeded by a relatively thin neck (the "dinuclear regime"), I will use the inertia appropriate to two *non*-communicating pieces (e.g., just a reduced mass for the relative motion of the mass centers). For shapes without a pronounced neck (the "mononuclear regime"), I will disregard the inertial forces entirely, for there is reason to believe that, in this regime, they are usually small compared to one-body dissipative forces. So this is the physics that will go into my machinery:

1. Macroscopic potential energy,
2. Macroscopic dissipation function,
3. Dinuclear inertia in the dinuclear regime and zero in the mononuclear regime.

I will make a schematic division between the mononuclear regime and the dinuclear regime at the point where the window through which the two pieces communicate is half open. The precise meaning of this will become clear after I have described the shape parametrization that I will use.

3. Shape parametrization

In striving for an algebraic theory of a complex process, the choice of appropriate and elegant degrees of freedom is half the battle. Figure 1 shows the best I could do to date: two spheres with radii R_1, R_2 and center separation r, connected by a portion of a cone with semiopening angle θ. There are three degrees of freedom (the absolute minimum required to describe the type of processes we are after). They are

1. Asymmetry variable $\Delta = \dfrac{R_1 - R_2}{R_1 + R_2}$ (1)

2. Distance variable $\rho = \dfrac{r}{R_1 + R_2}$ (2)

3. Window-opening variable $\alpha = \left(\dfrac{\sin\theta}{\sin\theta_{max}}\right)^2$. (3)

Here $\sin\theta_{max}$, equal to $(R_1 - R_2)/r$, refers to a fully open window, so that α, which ranges from 0 to 1, is a measure of the degree of communication between the two pieces. I shall take $\alpha = \frac{1}{2}$ to be the boundary between the dinuclear and mononuclear regimes.

4. The configuration space

The variable Δ ranges from -1 to +1, α ranges from 0 to 1, and ρ from 0 to ∞, so the configuration space is a semi-infinite box, shown in perspective in Fig. 2 and in plan and side view in Fig. 3. The box is bounded by the horizontal planes $\alpha = 0, 1$, by the vertical planes $\Delta = -1, +1$ (only the positive half of the box is shown in Fig. 2), and by a curved surface on the left, corresponding to the minimum window that has to be there when the two spheres intersect. (The volume is always considered renormalized, so there is no implied density doubling anywhere.) The configuration box is a little like a semi-infinite aircraft carrier steaming to the left. The shapes corresponding to various parts of the box are indicated by descriptive labels. The single sphere is anywhere along and to the left of the diagonal lines $\rho = \pm\Delta$ on the overhanging part of the flight deck, where the larger of the two spheres has swallowed up entirely the smaller one. Proceeding along the deck to the right results in more and more elongated conical frustums, capped with spheres. The shapes are reflection symmetric along the ship's midplane. As one descends toward the waterline, the shapes become necked-in. Separating spheres are at the waterline to the right. The aircraft carrier's curved stem corresponds to intersecting spheres.

This then is the layout of the configuration box that will act as the stage for the various dynamical trajectories corresponding to two nuclei coming together, interacting, and either ending as a single sphere on the left or reseparating as two pieces on the right.

5. The potential energy

The macroscopic potential energy is the usual sum of surface and Coulomb energies. I have found a simple and useful parametrization of the potential-energy surface by starting with an expansion to third order in the neck size, written in terms of a set of special "elegant variables" ν and σ. These variables are defined in terms of α and ρ by

$$\nu \equiv \sqrt{\alpha} \qquad \text{(range 0 to 1)}\ , \tag{4}$$

$$\sigma \equiv \frac{\rho^2 - 1}{1 - \Delta^2} \qquad \text{(range } -1 \text{ to } \infty\text{)}. \tag{5}$$

For a small neck, ν reduces to the neck radius in units of twice the "reduced radius" $\bar{R}$ of the system ($\bar{R} = R_1 R_2/(R_1 + R_2)$):

$$\nu \rightarrow \frac{\text{neck radius}}{2\bar{R}}\ . \tag{6}$$

Similarly, σ tends to the tip separation of the spheres in units of $2\bar{R}$:

$$\sigma \rightarrow \frac{\text{tip separation}}{2\bar{R}}\ . \tag{7}$$

As the configuration tends to a sphere (i.e., $\rho \rightarrow \pm\Delta$), σ tends to -1.

In terms of these variables, the potential energy, taken with respect to the energy of tangent spheres and written in units of the quantity $8\pi\bar{R}^2\gamma$, may be approximated by the following cubic:

$$\eta \equiv \frac{PE - PE_{tg}}{8\pi\bar{R}^2\gamma} = \nu\sigma - \nu^2 + \nu^3 - X\sigma\ . \tag{8}$$

Here X is an "effective fissility parameter" given by

$$X = \frac{Z_1 Z_2 e^2/(R_1 + R_2)^2}{4\pi\gamma\bar{R}} \quad , \tag{9}$$

where $Z_1 e, Z_2 e$ are the electric charges on the two pieces and γ is the surface-energy coefficient. This "effective fissility parameter" X is analogous to the usual fissility parameter and is a measure, for dinuclear systems, of the importance of the repulsive electric force $Z_1 Z_2 e^2/(R_1+R_2)^2$ compared to the attractive nuclear surface-tension or "proximity" force $4\pi\bar{R}\gamma$. For a system with a given mass number, the dependence of X on asymmetry is readily verified to be

$$X = X_o \frac{(1-D)^2}{1+3D} \quad , \tag{10}$$

where

$$X_o = \frac{Z^2 e^2}{16\pi\gamma R^3} \quad , \tag{11}$$

$$D = \Delta^2 \quad , \tag{12}$$

and Ze,R refer to the charge and radius of the combined system. The fissility parameter X_o is identical, apart from a factor, with the usual fissility parameter x defined by $3Z^2e^2/40\pi\gamma R^3$.

6. Conditional and unconditional saddle points

The configurations where the potential energy η is stationary with respect to all small variations of Δ, ρ, α are true (unconditional) saddles, of which the symmetric Bohr-Wheeler and asymmetric Businaro-Gallone saddles are the most important.

Configurations where η is stationary with respect to ρ,α *when the asymmetry* Δ *is frozen* are also important in the dinuclear regime where the asymmetry degree of freedom is inhibited to a greater or lesser extent. These are "conditional" saddles, the equilibrium being conditional on the inhibition of the asymmetry. For the location $\bar{\nu}$, $\bar{\sigma}$ of a conditional saddle one finds, by differentiation of Eq. (8),

$$\bar{\nu} = X \quad , \tag{13}$$

$$\bar{\sigma} = 2\bar{\nu} - 3\bar{\nu}^2 = 2X - 3X^2 \quad . \tag{14}$$

The saddle-point energy follows as

$$\eta(\bar{\nu},\bar{\sigma}) = -X^2 + X^3 \quad . \tag{15}$$

One recognizes here a useful static scaling rule of our model:

"The dimensionless conditional saddle-point properties (such as the relative degree of window opening and the energy deviation from tangent spheres expressed in unts of $8\pi\bar{R}^2\gamma$*) are functions of the effective fissility parameter* X *alone, and independent of asymmetry."*

For symmetric systems, the conditional saddles become the unconditional Bohr-Wheeler saddles, since the frozen-asymmetry condition is then redundant.

Because our energy expression for η is relatively simple, the properties of all the saddle points, including the Businaro-Gallone asymmetric shapes, can be written down in closed form. For example, the fission-barrier energy (the energy of the Bohr-Wheeler saddles), in units of the surface energy of the spherical shape, follows as

$$\xi = \frac{PE - PE_{sphere}}{4\pi R^2 \gamma} = a - bX_o - cX_o^2 + cX_o^3 \quad , \qquad (16)$$

where

$$a = 2^{1/3} - 1 = 0.259921 \quad ,$$

$$b = \frac{12}{5} - \frac{17}{10} 2^{1/3} = 0.258134 \quad ,$$

$$c = 2^{-5/3} = 0.314980 \quad .$$

Equation (16) is compared with an accurate computer calculation [1] in Fig. 4. In the present approximation, the Bohr-Wheeler family of symmetric saddle-point shapes starts as tangent spheres at $X_o = 0$, elongates until $X_o = 1/3$, then contracts to become, at $X_o = 2/3$, a pair of tangent spheres connected by a neck that is four-ninths open, and finally becomes a single sphere at $X_o = 1$. The degree of opening of the neck (window) is $\frac{1}{2}$ when $X_o = 1/\sqrt{2} \approx 0.7$. All this is roughly in agreement with exact calculations, especially if the fissility parameter X_o is taken to be defined not in terms of fundamental constants through Eq. (11), but as the "relative fissility," i.e., the value of the charge on the system divided by that critical value which makes the Bohr-Wheeler saddle-point (in the model in question) coincide with the sphere (and causes the fission barrier to vanish or nearly vanish). We may then make the following identifications:

$$X_o \leftrightarrow x = \frac{3Z^2 e^2}{40\pi\gamma R^3} \quad , \qquad (17)$$

$$X \leftrightarrow x_{eff} = \frac{3Z_1 Z_2 e^2/(R_1 + R_2)^2}{10\pi\gamma\bar{R}} = x \frac{(1-D)^2}{1+3D} \quad . \qquad (18)$$

These equations differ by a factor 6/5 from Eqs. (9) and (11). The above implicit definition of X_o and the identication of X_o with x underlies the plot in Fig. 4. Figure 4 also shows the asymmetric Businaro-Gallone saddles peeling off at the point $(X_o)_{BG}$, given by

$$(X_o)_{BG} = \frac{14}{57} + \frac{4\sqrt{163}}{57} \cos\left(60° + \frac{1}{3}\cos^{-1}\frac{3587}{652\sqrt{163}}\right)$$

$$= 0.378174 \quad , \tag{19}$$

to be compared with the correct value $x_{BG} = 0.39_6$. The energy of the Businaro-Gallone shapes is also compared with the results of computer calculations in Fig. 4.

All in all it would seem that the energy expression for η, Eq. (8), inspired by a third-order expansion in the neck size, when expressed in terms of the "elegant variables" ν, σ, continues to provide a rough parameterization of the potential-energy surface all the way up to the spherical shape.

7. The dissipation function

This is a crucial physical ingredient in our study and it governs the overall character of the dynamics. I started from the Wall Formula for the rate of energy dissipation $\dot{Q}$ in the mononuclear regime and the Wall-and-Window formula in the dinuclear regime. The Wall formula reads as follows [2]:

$$\dot{Q} = \bar{\rho v} \oint (\dot{n} - D)^2 \, d\sigma \quad . \tag{20}$$

The Wall-and-Window formula is given by [3]:

$$\dot{Q} = \tfrac{1}{4}\,\rho\bar{v}\cdot\Delta\sigma\cdot(u_t^2 + 2u_r^2) + \rho\bar{v}\oint_{\text{fragment 1}}(\dot{n} - D_1)^2 d\sigma + \rho\bar{v}\oint_{\text{fragment 2}}(\dot{n} - D_2)^2 d\sigma \quad . \tag{21}$$

Here ρ is the nuclear mass density, $\bar{v}$ is the mean nucleonic speed, $\dot{n}$ is the normal velocity of a surface element $d\sigma$, $\Delta\sigma$ is the area of the window, and u_t, u_r are the tangential and radial components of the relative motion of the two pieces. The quantity D (not to be confused with Δ^2 in Eq. (10)) is a "normal drift velocity component" of the particles about to strike a surface element. It ensures the conservation of linear (and angular) momentum. (Without D, a uniformly translating nucleus would be losing energy.) Under a certain assumption, discussed in [2], D becomes a known function of the configuration and its state of motion, so that the integrals in Eqs. (20) and (21) can be evaluated.

As in the case of the potential energy, I used expansions of Eqs. (20,21) to cubic order in the neck size, expressed them in terms of the elegant variables ν, σ, and used the resulting equations for *all* neck sizes. For small necks, the resulting formulae may thus be expected to be semi-quantitative (within the other idealizations of the theory), but for large necks they are only qualitative.

8. The kinetic energy

For head-on collisions, I took the kinetic energy as

$$\mathrm{KE} = \begin{cases} \tfrac{1}{2} M_r \dot{r}^2 & \text{for } \alpha < \tfrac{1}{2} \\ 0 & \text{for } \alpha > \tfrac{1}{2} \end{cases} \quad . \tag{22}$$

Here M_r is the reduced mass of the separated fragments.

I shall comment on possible extensions to noncentral collisions later.

9. Equations of motion

In the dinuclear regime, the resulting equations of motion for ν,σ end up looking like this:

$$\mu \frac{d^2\sigma}{d\tau^2} + \nu^2 \frac{d\sigma}{d\tau} + \nu - X = 0 \quad , \tag{23}$$

$$\frac{d\nu}{d\tau} = \frac{2\nu - 3\nu^2 - \sigma}{\nu(\sigma + \nu^2)} \quad , \tag{24}$$

where

$$\tau = \frac{\text{time}}{t_u} \quad , \tag{25}$$

$$t_u = \text{natural time unit} = \frac{\rho\bar{v}\bar{R}^2}{\gamma} \quad , \tag{26}$$

and

$$\mu = \text{dimensionless reduced mass} = \frac{M_r}{2\pi(\rho\bar{v})^2\bar{R}^4/\gamma} \quad , \tag{27}$$

where $M_r = m\,A_1A_2/A$, with $m = 931\ \text{MeV}/c^2$. (A_1, A_2 are the mass numbers of the separated fragments and A is their sum.)

The structure of the equations of motion leads to the following dynamical scaling rule: *"For two dinuclear systems with the same values of the dimensionless reduced mass* μ *and of the effective fissility* X*, the dynamical evolutions resulting from head-on collisions should be similar, provided lengths are measured in units of (twice) the reduced radius* $\bar{R}$ *and times in units of* $\rho\bar{v}\bar{R}^2/\gamma$."

In practice, it will turn out that the dependence of dynamical calculations on μ is relatively slight for many systems of interest, so that the time evolutions of dinuclear systems should, in fact, be approximately similar provided only the effective fissilities X are the same.

In the mononuclear regime, the equations of motion are somewhat more complicated. The natural unit of length is then R and a natural unit of time is

$$t_o = \frac{\bar{\rho v} R^2}{4\gamma} \quad . \tag{28}$$

The single dimensionless parameter in the equations is the relative fissility X_o, since inertia is neglected.

Let us now look at some results.

10. Normal modes

The equations of motion are sufficiently simple so that approximate solutions in closed form may be found in several cases of interest. In particular, the normal modes of motion near the saddle points can be analyzed and explicit formulae for the characteristic times can be written down.

In the mononuclear regime there are three fully overdamped normal modes near the Bohr-Wheeler saddle. One is an exponentially growing fission mode with characteristic e-folding growth time T_f; the second is an exponentially decaying "transverse" mode with characteristic time T_t; and the third is the asymmetric mode with characteristic time T_Δ. In the dinuclear regime there are two modes: an exponentially

growing fission mode, as before, and an oscillating transverse mode with a characteristic time T_{osc} (i.e., with a *period* $2\pi T_{osc}$) and a characteristic damping time T_t.

The three characteristic times T_f, T_t, T_Δ, or T_f, T_{osc}, T_t are shown as functions of X_o in Fig. 5. The scale on the left is in units of 10^{-22} sec. On the right is a scale in MeV for the quantities $\hbar/T$.

Note the following qualitative features: The characteristic time for the fission mode changes by more than an order of magnitude from values $\sim 10^{-22}$ sec for light nuclei to a few times 10^{-21} sec for heavy nuclei. The asymmetry mode has a similarly sluggish time scale for heavy nuclei. For lighter nuclei, the (stable) asymmetry mode is inhibited by the neck constriction and, moreover, its restoring force tends to zero at the Businaro-Gallone point $(X_o)_{BG}$. Its characteristic decay time tends, therefore, to ∞ as X_o tends to ~ 0.4. All this suggests that the characteristic time for the asymmetry mode (when $X_o > 0.4$) may always remain fairly long (e.g., in excess of about one or a few times 10^{-22} sec).

The characteristic time of the overdamped transverse mode is much shorter than that of the fission mode for heavy nuclei. For lighter nuclei, the transverse mode has a damped oscillatory character which, for very light systems, should, in fact, have only moderate or even small damping. The transverse mode in those cases consists of a stable to and fro oscillation of the two pieces, with an associated swelling and contraction of the neck, which might also be described as a giant quadrupole resonance of the saddle shape, or as a quasimolecular mode. The energy of this resonance for light nuclei might be several MeV or even in excess of 10 MeV for the lightest systems (see Fig. 5).

11. Dinucleus (deep-inelastic), mononucleus (quasifission) and capture (compound-nucleus) reactions

Figure 6 shows three dynamical trajectories for a collision between two mass-104 nuclei at three energies: 0, 3.6 and 10 MeV above the interaction barrier. The total system has $A \approx 208$ and $Z \approx 82$, which corresponds to a fissility $X_o = 0.7$. [In all the examples I will show, the total system is chosen to be on the valley of beta-stability, with $N-Z = 0.4A/(A+200)$]. The reaction is symmetric, so everything happens in the midplane of the configuration box, at $\Delta = 0$. Figure 6 shows some of the equipotential lines which delineate the saddle point whose energy is 0.033 in units of the surface energy $4\pi R^2\gamma$. This corresponds to a fission barrier of some 19 MeV. The approach of the two nuclei corresponds to a trajectory along the ρ-axis, moving from right to left. At the point $\rho = 1.0$, the two spheres touch, and the first curve shows the subsequent dynamical evolution in the case where there is zero energy in excess of the barrier.

The dots on the trajectory mark equal intervals of time corresponding to 1/10 of the natural time unit $\rho\bar{\nu}R^2/4\gamma$. In the present case this unit is 12×10^{-22} sec, so the time between dots is 1.2×10^{-22} sec.

Note the very rapid initial growth of the neck, the leveling out, and the subsequent approximately linear decrease in the *neck area* (the variable α is proportional to the area). This means that the neck radius, proportional to $\sqrt{\alpha}$, snaps with a vertical tangent. The whole reaction lasts about 16×10^{-22} sec from contact to snapping, and it takes place entirely outside the saddle point. Even so, some energy has been dissipated during the neck growth and collapse, and the two

fragments would have less energy at infinity than that corresponding to the interaction barrier, which is what they started with.

The second trajectory in Fig. 6, with 3.6 MeV above the barrier at injection, also fails to be captured inside the saddle, although it hovers just outside it for a somewhat longer time. The third trajectory, with 10 MeV, gets captured easily, enters the mononuclear regime, and then creeps toward the spherical shape.

We thus see two distinct classes of reactions or trajectories: trapping and nontrapping ones, leading to a compound nucleus and a dinucleus respectively. The latter process would probably be recognized as a deep-inelastic reaction. In addition, there would, of course, be elastic reactions that never established proper nuclear contact, and quasielastic reactions, which the present model is too crude to bring out as a separate type.

The above situation changes drastically if one goes to lighter (symmetric) systems with lower values of the fissility X_o (see Fig. 7 for an example of a system with $X_o = 0.4$). The saddle point for a light system has $\rho > 1$, i.e., the saddle shape is more elongated than tangent spheres. Hence, after contact and neck growth, the system finds itself comfortably inside the saddle and heads without hesitation toward the spherical compound nucleus. There will still be elastic and quasielastic reactions, but the deep inelastic reactions will have disappeared(in head-on collisions).

The opposite happens if one goes to heavier systems, with higher values of X_o. Figure 8 shows a case with $X_o = 1$, corresponding to a super-heavy system with $A \approx 320$, $Z \approx 120$. In trying to make such a super-

heavy nucleus by colliding two equal pieces with $A_1 = A_2 = 160$, $Z_1 = Z_2 = 60$, one is faced with a potential-energy landscape that slopes monotonically away from the spherical configuration on the left. The trajectory shown corresponds to starting with zero kinetic energy at the barrier and, clearly, one never even gets close to the spherical configuration (where a compound-nucleus pocket might exist because of shell effects).

In the present model, the critical fissility X_c above which, for the first time, a compound nucleus refuses to form automatically (and deep-inelastic reactions would be expected to make their appearance in head-on collisions), turns out to be about 0.57. Recall that the saddle is more or less as compact as the tangent configuration at $X_o = 2/3 \approx 0.67$. The difference between 0.67 and 0.57 is a reflection of the fact that during neck growth the fragments begin to separate and, consequently, in order to achieve capture, the contact configuration must be somewhat more compact than the saddle, i.e., X_o must be somewhat less than 2/3.

Two things can be done if one has a system with $X_o > X_c$ and one nevertheless wants a compound nucleus. The first is to increase the bombarding energy, as already illustrated in Fig. 6. This works if X_o is not too much above X_c. The other possibility is to go to an *asymmetric* target-projectile combination. A dramatic illustration of this is provided by Fig. 9. Here we have the same super-heavy system (with $X_o = 1$, $A \approx 320$) as before, but the asymmetry is very large, with $A_1 \approx 296$, $Z_1 \approx 111$, and $A_2 \approx 24$, $Z_2 \approx 9$. (This corresponds to $\Delta = 0.4$.) The *effective* fissility is now only $X = 0.4768$. This means that in

the dinuclear regime, the system behaves like a much lighter and less fissile nucleus. The equipotential lines in Fig. 9, displayed for a section at $\Delta = 0.4$, show the location of the *conditional* saddle point, which is now less compact than the tangent configuration (contrast this with the true saddle, all the way to the left). As a result, the trajectory starting with zero kinetic energy at the top of the barrier has now no difficulty in being captured and proceeds toward the left. After it has entered the mononuclear regime, the asymmetry gets unfrozen and begins to increase somewhat, as shown in the upper part of Fig. 9. This makes little difference and the spherical configuration is attained without difficulty in about one time unit.

If, with X_o fixed at 1, the asymmetry is made less extreme, the automatic capture eventually comes to an end. It turns out that this coincides with the point when capture inside the *conditional* saddle fails to take place, for X less than about 0.57. The asymmetry Δ of that point is given by solving $0.57 \approx (1-D)^2/(1+3D)$, which leads to $\Delta \approx 0.346$ and $A_1 \approx 287$, $Z_1 \approx 108$ and $A_2 \approx 33$, $Z_2 \approx 12$ (see Fig. 10).

By carrying out a variety of such trajectory calculations for systems with different fissilities and asymmetries, one learns an interesting fact: the condition for automatic capture inside the conditional saddle is, to a fair approximation, simply that the *effective* fissility X should be less than X_c, with X_c estimated as roughly 0.57. (This is in accordance with our approximate dynamic scaling rule resulting from neglecting the relatively slight dependence on μ). Moreover, this scaling rule also suggests that when X is somewhat above X_c the extra push, or extra velocity above the barrier needed

for capture inside the conditional saddle, should be a function of $X - X_c$ only and, in fact, should have the following appearance:

$$\left(\frac{d\sigma}{d\tau}\right)_{crit} = -a(X - X_c) + \text{higher powers of } (X - X_c) \quad . \qquad (29)$$

Figure 11 illustrates the usefulness of this equation: the dots represent the results of a number of calculations of the critical injection velocity for a variety of systems with different fissilities X_o and different asymmetries. A straight line, with $a \approx 5$, $X_c \approx 0.57$, represents the results fairly well when X is close to X_c. (The scatter of the points reflects the slight dependence on μ.) When the dimensionless variables σ, τ and the effective fissility X (or x_{eff}) are written out in terms of the charge and mass numbers of the nuclei in question, the innocent looking Eq. (29) is equivalent to the following nontrivial statement: "The square root of the extra energy over the barrier needed to ensure capture inside the conditional saddle, when multiplied by the weird combination $A^{1/2}A_1^{-1/6}A_2^{-1/6}(A_1^{1/3} + A_2^{1/3})^{-1}$, should be approximately linear when plotted against the weird combination $Z_1Z_2A_1^{-1/3}A_2^{-1/3}(A_1^{1/3} + A_2^{1/3})^{-1}$."

In other words,

$$\sqrt{KE/MeV} \cdot \frac{\sqrt{A}}{A_1^{1/6}A_2^{1/6}(A_1^{1/3} + A_2^{1/3})} = C_1\left[\left(\frac{Z^2}{A}\right)_{eff} - C_2\right], \qquad (30)$$

where we have introduced the definition

$$\left(\frac{Z^2}{A}\right)_{eff} \equiv \frac{4Z_1Z_2}{A_1^{1/3}A_2^{1/3}(A_1^{1/3} + A_2^{1/3})} \quad , \qquad (31)$$

and C_1, C_2 are essentially constants given by

$$C_1 = \frac{4\sqrt{2}}{45}\left(\frac{3}{\pi}\right)^{1/3}\frac{e^2}{\hbar c}\sqrt{\frac{mc^2}{MeV}}\,a \qquad (32)$$

$$\approx \frac{1}{7}\,, \text{ if } a \approx 5 \text{ is taken as suggested by the present schematic calculations and}$$

$$C_2 = \frac{40\pi r_o^3 \gamma}{3} X_c = \left(\frac{Z^2}{A}\right)_{\text{eff crit}} \qquad (33)$$

$$\approx 26\text{-}27, \text{ if } 0.57 \text{ is taken as the estimate for } X_c.$$

The functional form of Eq. (30) follows on dimensional grounds from the structure of the equations of motion; the actual values of the slope C_1 and intercept C_1C_2 carry quantitative information on the magnitude of the dissipation in the dinuclear regime and could eventually provide a test of the window formula.

Figure 12 shows loci of equal values of the effective fissility X in a plot of the asymmetry Δ against the fissility X_o. For $X \lesssim 0.57$, automatic capture into a compound nucleus takes place. For $X \gtrsim 0.57$, an extra push, described by Eq. (29) or (30), is required for capture inside the conditional saddle. (The conditional saddle moves into the mononuclear regime at $X = 1/\sqrt{2}$, and Eq. (29) becomes a lower limit only.) Figure 13 is a translation of Fig. 12 from the space of fissility and asymmetry to the essentially equivalent space of A_1 and A_2. The contour lines indicate the extra push in MeV needed to make a pair of nuclei with mass numbers A_1, A_2 fuse beyond the conditional saddle.

Note the critical zero-push contour, below which automatic capture into a compound nucleus takes place. With a mass-40 projectile, there should be no serious problem in making a compound nucleus in a head-on collision with any target in the Periodic Table, except possibly the heaviest. With equal-mass reactions, increasing difficulties would be expected with projectiles heavier than about Kr.

Beyond the 15-20 MeV contour, the conditional saddle enters the mononuclear regime. Now when a trajectory enters this regime, the asymmetry gets unfrozen and a qualitatively new type of reaction may take place, as illustrated by Fig. 14. Here again we have $X_o = 1$ and the asymmetry is 0.3, so automatic capture does not take place (first trajectory). But with a push of 5 MeV, capture inside the conditional saddle takes place and one might have thought that a compound nucleus would result. But look what happens: after beginning to head for home, the trajectory enters the mononuclear regime, and the asymmetry begins to decrease. This results in an increasing Coulomb repulsion (Z_1Z_2 increases), and the trajectory turns around and heads out again. But because such a reversal has to wait for a change in asymmetry, which is a relatively slow process, the time for reseparation is about 3 times longer than in the case of the first trajectory (about 50×10^{-22} sec in absolute value). So even after capture inside the conditional saddle, there was no capture inside the true saddle and no compound-nucleus formation. By ramming with a higher energy (third trajectory, 45 MeV) a compound nucleus can be formed, but there will be a range of energies where capture inside the conditional but not inside the true saddle takes place. Such reactions

could be called mononucleus reactions. An example of an even longer-lived mononucleus reaction is shown in Fig. 15. Here $X_o = 0.9$, $\Delta = 0.2$, and the injection takes place with 67 MeV above the barrier, which easily ensures capture inside the conditional saddle. At first the trajectory heads for home, but after entrance into the mononuclear regime, it is a competition between the growing compactness of the configuration and the increasing Z_1Z_2 repulsion. The latter wins, but the total time for the reaction is now more than 8 units (more than 120×10^{-22} sec). By that time the asymmetry has drifted practically to zero and the reseparation is into two almost equal pieces. It would probably be very difficult to distinguish such a reaction from the fission of the compound nucleus and "quasifission" might be an appropriate term in this case.

Figure 16 provides another example of dinucleus (deep-inelastic), mononucleus (quasifission) and compound-nucleus reactions. In addition it shows a critical trajectory, with an injection energy close to 16.4 MeV, which would end up at rest at the saddle point, in a state of unstable equilibrium.

The above studies suggest the usefulness of distinguishing between the following regions of configuration space:

1. Compound-nucleus region. The region of the potential energy hollow around the ground state, bounded by the hypersurface in configuration space on which the potential energy is equal to the energy of the fission barrier.

2. Composite-nucleus or mononucleus region. The region outside the compound nucleus region but inside the region where there is a serious neck constriction (e.g., inside a somewhat fuzzy hypersurface

where the window is about half-open.)

3. Dinucleus region. The region where there is a serious neck constriction (e.g., where the window is less than about half open), but inside the scission hypersurface (this could be defined as the hypersurface where the half-density contour is about to become separated into two, or more, closed surfaces).

4. The separated region. The region outside the scission hypersurface.

In many cases one will probably find a fair correspondence between these four regions and the four types of reactions designated as

1. Compound
2. Quasi-fission
3. Deep-inelastic
4. Quasi-elastic and elastic.

One should remember, however, that only if a system is sufficiently heavy can one expect to see deep-inelastic reactions, and that only if the asymmetry is large enough can one expect the emergence of quasifission reactions as a somewhat distinct category from deep-inelastic reactions. This is because for symmetric systems there is only one saddle to overcome — the unconditional one — and trajectories that are not captured inside it will show a gradual shading of deep-inelastic into quasifission reactions. On the other hand, for sufficiently asymmetric systems, where the conditional saddle is in the dinuclear regime, one may expect a rough distinction between quasifission and deep-inelastic reactions related to the division of the trajectories into those that were or were not captured inside the conditional saddle.

12. Noncentral collisions

If only a small amount of angular momentum is present, the description given above for the time-development of the reaction in the degrees of freedom ρ, Δ, α would continue to be approximately valid provided the proper injection velocity in the distance degree of freedom (ρ) was used as the initial condition. This approximation corresponds to treating the centrifugal and Coriolis forces, as regards their effects on the dynamical development of the shape, as negligible compared to the electric and nuclear forces.

When the amount of angular momentum is large, some limited progress might be made in a simplified scheme where the centrifugal force was retained, but the Coriolis forces still disregarded. One could then try to mock up the centrifugal force by an increase in the electric repulsion, i.e., by the replacement of the effective fissility X by an effective disruption parameter χ defined by

$$\frac{\chi}{X} = 1 + \frac{\text{Centrifugal Force (near contact)}}{\text{Electric Force (near contact)}}$$

$$= 1 + \frac{L^2 M_r (R_1 + R_2)^3}{\mathcal{I}_o^2 Z_1 Z_2 e^2} \quad ,$$

where L is the angular momentum and $\mathcal{I}_o$ is an estimate of the moment of inertia near contact. This suggests the following generalized approximate scaling rule:

"For two dinuclear systems, with possibly different sizes, asymmetries and angular momenta, the dynamical time evolutions in a limited regime can be approximately scaled into each other (by the use of the

natural units of time and length) provided the effective disruption parameters χ are the same."

I intend to study further the usefulness of this approach (see also [3]).

13. Summary

I have sketched an attempt to develop an algebraic theory of the gross macroscopic dynamical shape evolutions in fission and nucleus-nucleus collisions. A crucial physical ingredient was the one-body dissipation function. Even though the price paid for an algebraic theory was the introduction of various more or less drastic technical approximations (that could, in principle, be avoided), the scheme may be useful in suggesting scaling rules and making more precise our intuitive ideas about various types of reactions (deep-inelastic, quasifission, compound-nucleus). There is a wealth of specific information in these studies on normal modes, on reaction times, on energy loss, etc., which I have not been able to present, and the treatment of angular momentum has not progressed very far. Also, I have not been able to give a comparison with experimental evidence, but I look forward to a broad confrontation of theory and experiment in the future. I hope the scheme I have described may prove to be a useful background and a complement to more detailed and realistic microscopic computer studies of the kind that Sven-Gösta Nilsson and his Lund Group were masters of.

Acknowledgment

This report was prepared by the Nuclear Science Division of the Lawrence Berkeley Laboratory under the University of California contract W-7405-ENG-48 with the U.S. Department of Energy.

References

1. Cohen,S. and Swiatecki,W.J., Ann. Phys. 22, 406 (1963); Blocki,J., Randrup,J., Swiatecki,W.J. and Tsang,C.F., Ann. Phys. 105, 427 (1977) and references therein.

2. Randrup,J. and Swiatecki,W.J., Ann. Phys. 124, 193 (1980) and references therein; Blocki,J., Boneh,Y., Nix,J.R., Randrup,J., Robel,M., Sierk,A.J. and Swiatecki,W.J., Ann. Phys. 113, 338 (1978). See also [3].

3. Swiatecki,W.J., Three lectures on macroscopic aspects of nuclear dynamics, presented at International School of Nuclear Physics, "Ettore Majorana" Center for Scientific Culture, Erice-Trapani, Sicily, March-April 1979, to be published in Proceedings (D.Wilkinson, ed.), also Lawrence Berkeley Laboratory preprint LBL-8950, March 1979.

Figure captions

Fig. 1. The nuclear configuration is parametrized by two spheres connected by a conical neck. The asymmetry is specified by Δ, the center-separation by ρ, and the degree of window opening by α. The distance between the tips of the spheres may be positive or negative.

Fig. 2. Perspective view of half the "configuration box" (corresponding to $\Delta > 0$). The part shown is bounded by the planes $\alpha = 0,1$ and $\Delta = 0,1$. A curved surface bounds the box on the left. On the right, the box extends to infinity. Various types of shapes correspond to the different parts of the box, as indicated by descriptive labels. In the dinuclear regime, the approximation is made that the configuration space is a stack of noncommunicating sections at fixed asymmetry.

Fig. 3. Plan and side view of the configuration box from Fig. 2. The side view suggests a similarity of the box with the shape of an aircraft carrier. The flight deck is carried forward on a curved bow and overhangs the hull in the triangular regions labeled "single sphere." The two spheres describing the shape are tangent at $\rho = 0$. "Half-immersion" corresponds to shapes where the center of the smaller sphere has just entered the larger sphere. Full immersion takes place for $\Delta < \rho$ and leads to a single sphere for the resulting shape.

Fig. 4. Comparison of the energies of the Bohr-Wheeler and Businaro-Gallone saddles as calculated in our approximation (using a cubic potential energy) with accurate values calculated with the aid of electronic computers. The relative fissility X_o or x may be regarded as the charge on the system, divided by the value that makes the Bohr-Wheeler saddle spherical. The critical bifurcation point, where the Businaro-Gallone saddles branch off, is indicated by an arrow.

Fig. 5. The characteristic times of the normal modes of motion in the vicinity of the Bohr-Wheeler saddle. To the right of the shaded band, in the mononuclear regime, all the modes are overdamped, with exponential growth or decay times as shown. In the dinuclear regime, the fission mode is a growing exponential, and the transverse mode is an oscillation with angular frequency T_{osc}^{-1} and damping time T_t.

Fig. 6. Example of a dynamical study of symmetric collisions between two medium-weight nuclei ($A_1 = A_2 \approx 104$, $Z_1 = Z_2 \approx 41$). The total system is characterized by a fissility $X_o = 0.7$. The lower part of the figure gives a projection on the α-ρ plane and the upper part a projection on the Δ-ρ plane of the configuration space. The first and second trajectories, with energies 0 and 3.6 MeV above the interaction barrier, fail to fuse and reseparate after dissipating some energy. With 10 MeV above the barrier, fusion takes place (third trajectory). Dots are spaced at 1/10 of the natural time unit, i.e., at

1.2×10^{-22} sec. Circled dots indicate the lapse of a full time unit. The dashed lines are equipotentials, with energy expressed in units of the surface energy of a single sphere (about 583 MeV) and with reference to the energy of the spherical configurations. The location of the saddle point is indicated by the crossing equipotentials in the α-ρ plane and by a semicircle with a cross in the Δ-ρ plane (upper part of the figure). The asymmetry is specified by Δ on the left and by the fractional target mass on the right. The quantities S' are dimensionless injection velocities for the three trajectories.

Fig. 7. This is like Fig. 6 but refers to a lighter system with $X_o = 0.4$ ($A \approx 106$, $Z \approx 46$). The saddle-point shape is now more elongated than the tangent configuration and automatic capture into a compound nucleus takes place even with zero injection velocity. Note the discontinuity in the slope of the trajecotry at $\alpha = \frac{1}{2}$, which reflects the discontinuous transition from the dinuclear to the mononuclear regime.

Fig. 8. This is like Fig. 6 but for a super-heavy system with fissility $X_o = 1$ ($A \approx 320$, $Z \approx 120$). The saddle point (crossed circle) is now the sphere at $\rho = 0$, $\alpha = 1$. The trajectory with zero energy above the barrier never comes close the the spherical configuration.

Fig. 9. The total system is the same as in Fig. 7, but the asymmetry corresponds to $\Delta = 0.4$ ($A_1 \approx 296$, $Z_1 \approx 111$ and $A_2 \approx 24$, $Z_2 \approx 9$). The equipotentials refer now to a section at $\Delta = 0.4$ (and not

to the midplane $\Delta = 0$, as in Figs. 6 and 7). The conditional saddle is more elongated than the tangent configuration and automatic capture inside this saddle takes place. The system then proceeds to fuse and reaches the spherical shape without hesitation.

Fig. 10. This is similar to Fig. 8, but the asymmetry is $\Delta = 0.346077$ ($A_1 \approx 287$, $Z_1 \approx 108$; $A_2 \approx 33$, $Z_2 \approx 12$), which is close to the critical value below which automatic capture does not take place. The effective fissility is $X = 0.57$, and the trajectory only barely manages to be captured inside the conditional saddle. It hovers for about one time unit very close to the saddle.

Fig. 11. The critical injection velocity (in the natural unit $2\gamma/\rho v\bar{R}$) needed for capture inside the conditional saddle is plotted against the effective fissility X. Some 40 different reactions covering a wide range of target-projectile combinations, are represented by the dots. The fair degree of clustering of the dots in a plot vs. X attests to the relatively slight dependence of the trajectories in the dinuclear regime on the inertia parameter μ. For $X > 1/\sqrt{2}$, the conditional saddles enter the mononuclear regime and the continued use of equations of motion appropriate to the dinuclear regime can only provide a lower limit on the critical injection velocity. The dots followed from approximate analytic solutions of the equations of motion. The circles, obtained by numerical integrations, provide spot checks on the accuracy of those solutions.

Fig. 12. If nuclear reactions are classified according to the asymmetry Δ and the fissility X_o, the Δ-X_o plane becomes divided into two regions, with the effective fissility X less than or greater than X_c (equal to about 0.57 in the present model). For $X \gtrsim 0.57$, deep-inelastic reactions are expected to make their appearance in head-on collisions. For $X \gtrsim 1/\sqrt{2}$ the conditional saddles enter the mononuclear regime and tend to lose their physical significance because of the unfreezing of the asymmetry degree of freedom.

Fig. 13. This is a translation of the Δ vs. X_o diagram of Fig. 12 into a classification of reactions according to target and projectile mass numbers. The contour lines indicate estimates of the extra energy above the interaction barrier (in MeV) required for capture inside the conditional saddle. Below the zero-MeV contour, automatic capture takes place. Above a contour with 15-20 MeV, the conditional saddle is in the mononuclear regime and the dashed contours are then only lower limits. The circled numbers indicate the energy above the barrier (in MeV) required for compound-nucleus formation (or, in the case of the heaviest systems, for the attainment of the spherical shape). The triangle, circle, dot, and cross indicate approximately the locations of four superheavy-type reactions, listed on the right (together with estimated fission barriers due to hypothetical shell effects). Two other reactions (leading to the same compound nucleus with A = 215) are also indicated. The figure suggests that a direct

dynamical fusion of two comparable nuclei into a superheavy system is opposed by a huge "wall" requiring tens of even hundreds of MeV in excess of the interaction barrier. The height of the wall drops off precipitously as the asymmetry of the reaction is increased and might be tolerable by the time projectiles with a mass of $A_2 \approx 50$ are used. With projectiles below some mass in the range 30-40, automatic attainment of the spherical shape might be expected (the "end run" into the "superheavy end zone").

Fig. 14. This is like Figs. 6-10 but illustrates the emergence of mononucleus (quasifission) reactions as a species separate from dinucleus (deep-inelastic) reactions. The middle trajectory, with 5 MeV injection energy, is captured inside the conditional saddle but leads to reseparation after a decrease of the asymmetry.

Fig. 15. This is another example of a mononucleus reaction, where capture inside the conditional saddle took place but the unconditional saddle was not surmounted. This "quasi-fission" reaction took more than 120×10^{-22} sec and the final division is almost symmetric.

Fig. 16. This figure illustrates three types of reactions: (a) deep inelastic (lowest trajectory) following injection with zero energy above the barrier, (b) quasifission, following injection with 7.2 MeV (the other reseparating trajectory), and (c) a compound-nucleus reaction (trajectory on the left, with 65.7

MeV injection energy). The fourth curve corresponds to a critical injection energy close to 16.4 MeV, chosen so that the system would come to rest (in unstable equilibrium) at the unconditional saddle point (indicated by a crossed semicircle).

THE NUCLEAR CONFIGURATION AS SPECIFIED BY ③ DEGREES OF FREEDOM:

$$\text{ASYMMETRY } \Delta = \frac{R_1 - R_2}{R_1 + R_2}$$

$$\text{DISTANCE } \rho = \frac{r}{R_1 + R_2}$$

$$\text{WINDOW OPENING } \alpha = \left(\frac{\sin\theta}{\sin\theta_{max}} \right)^2$$

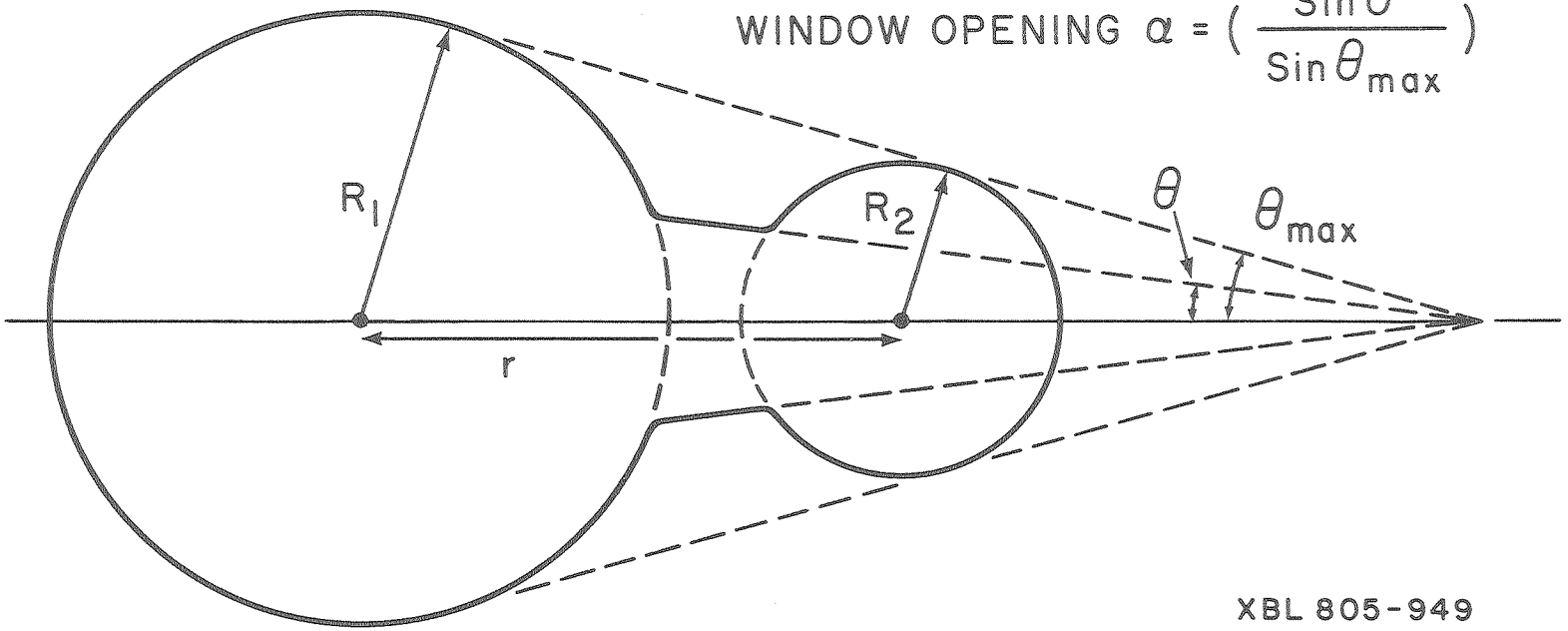

XBL 805-949

Fig. 1

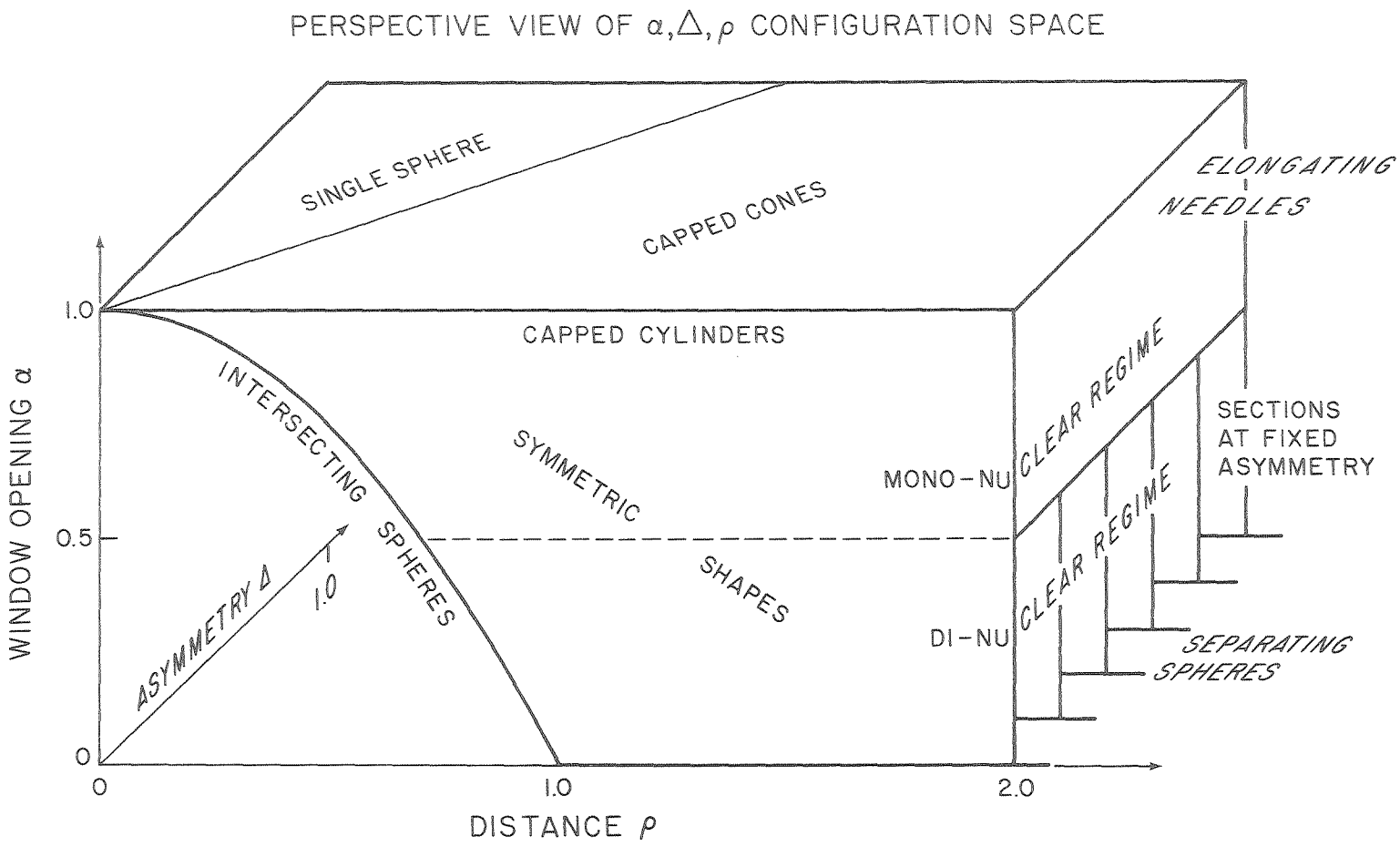
PERSPECTIVE VIEW OF α,Δ,ρ CONFIGURATION SPACE
SINGLE SPHERE
CAPPED CONES
ELONGATING NEEDLES
CAPPED CYLINDERS
INTERSECTING SPHERES
SYMMETRIC SHAPES
MONO-NU CLEAR REGIME
DI-NU CLEAR REGIME
SECTIONS AT FIXED ASYMMETRY
SEPARATING SPHERES
ASYMMETRY Δ
1.0
WINDOW OPENING α
1.0
0.5
0
0
1.0
2.0
DISTANCE ρ
XBL 805-952

Fig. 2

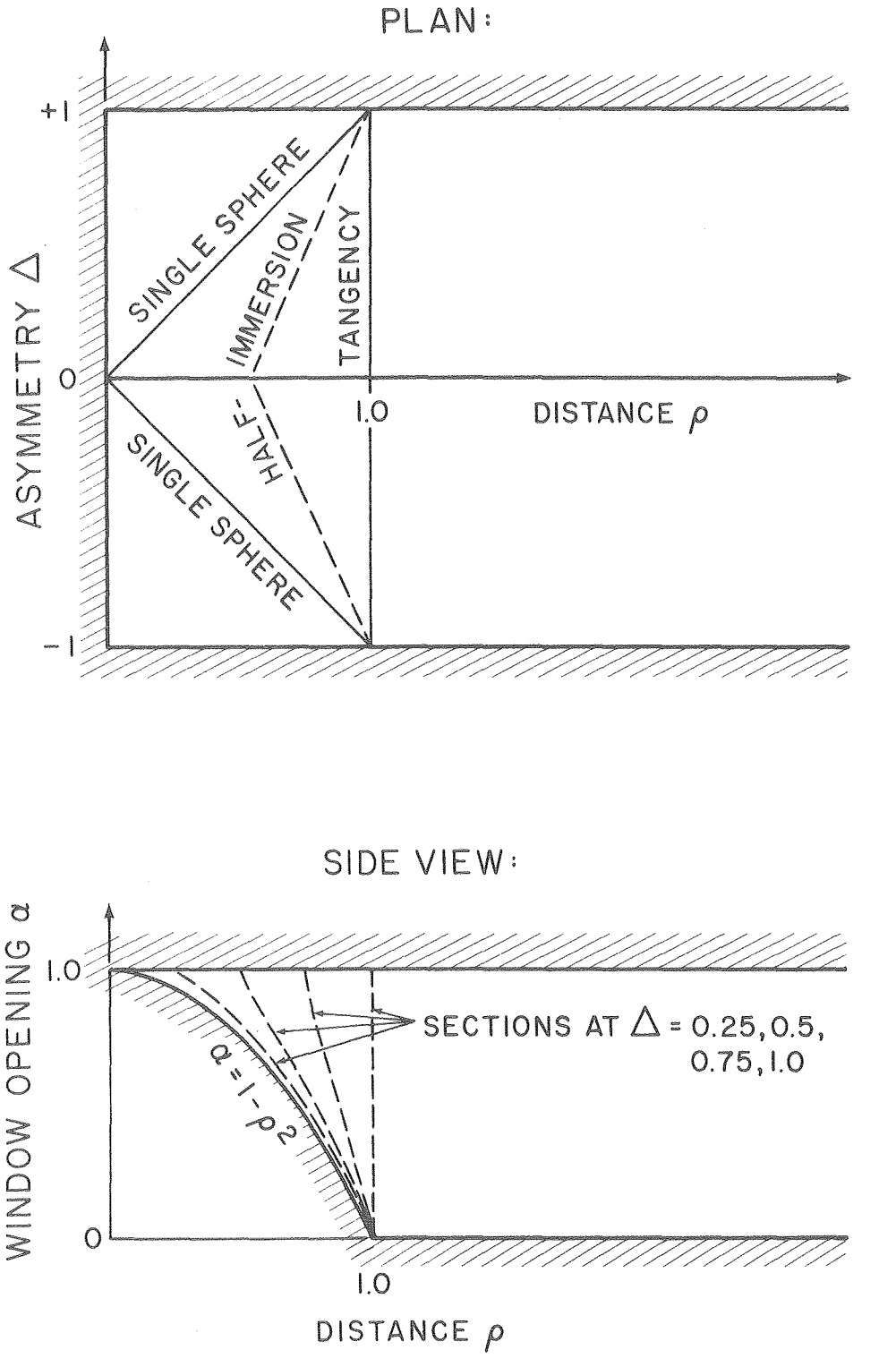
PLAN:
+1
ASYMMETRY Δ
0
-1
SINGLE SPHERE
IMMERSION
TANGENCY
HALF-
SINGLE SPHERE
1.0
DISTANCE ρ
SIDE VIEW:
WINDOW OPENING α
1.0
0
α = 1 - ρ²
SECTIONS AT Δ = 0.25, 0.5, 0.75, 1.0
1.0
DISTANCE ρ
XBL 805-948

Fig. 3

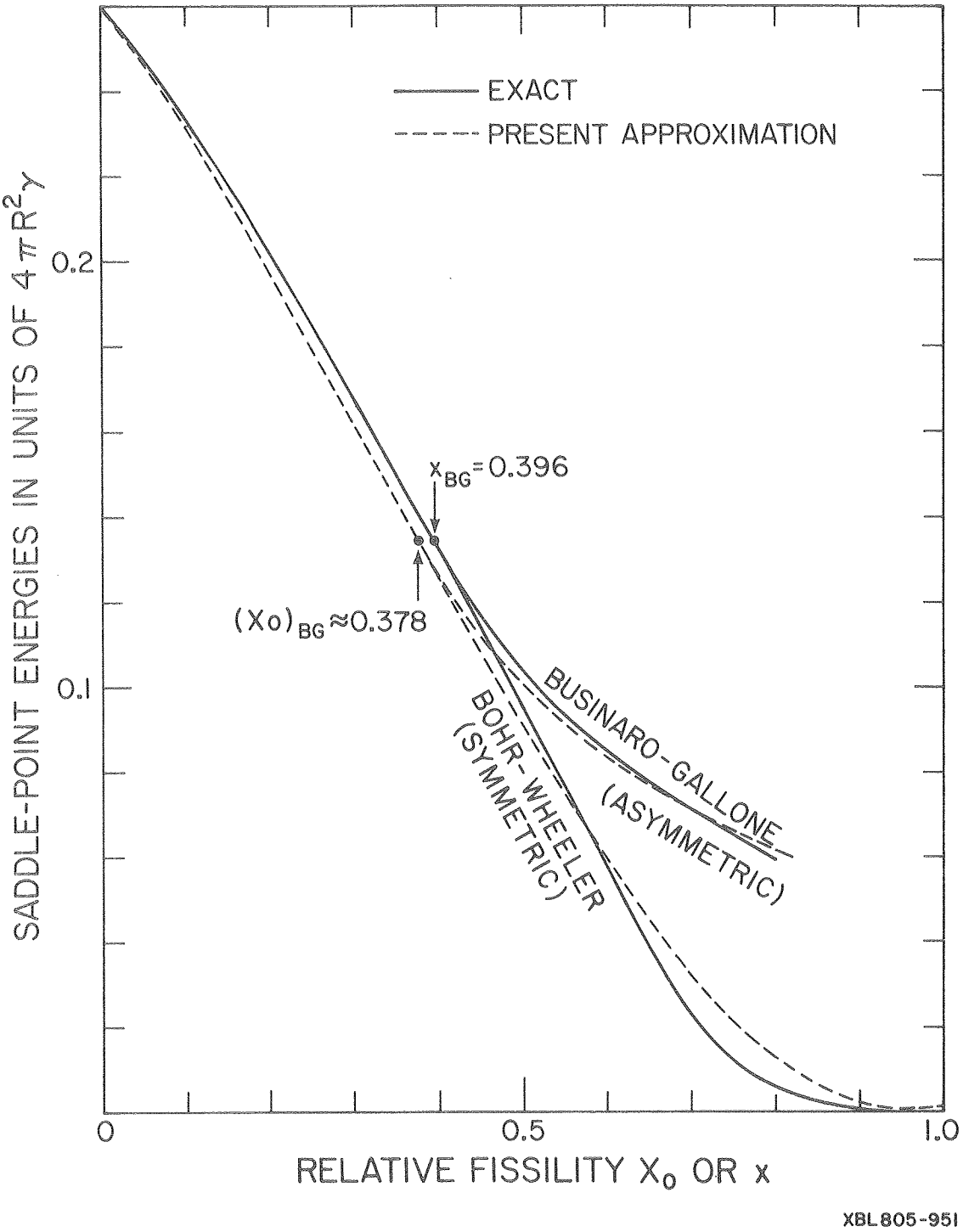
EXACT
PRESENT APPROXIMATION
x_{BG}=0.396
$(Xo)_{BG}$≈0.378
BUSINARO-GALLONE (ASYMMETRIC)
BOHR-WHEELER (SYMMETRIC)
SADDLE-POINT ENERGIES IN UNITS OF $4\pi R^2\gamma$
0.2
0.1
0
0.5
1.0
RELATIVE FISSILITY X_0 OR x
XBL805-951

Fig. 4

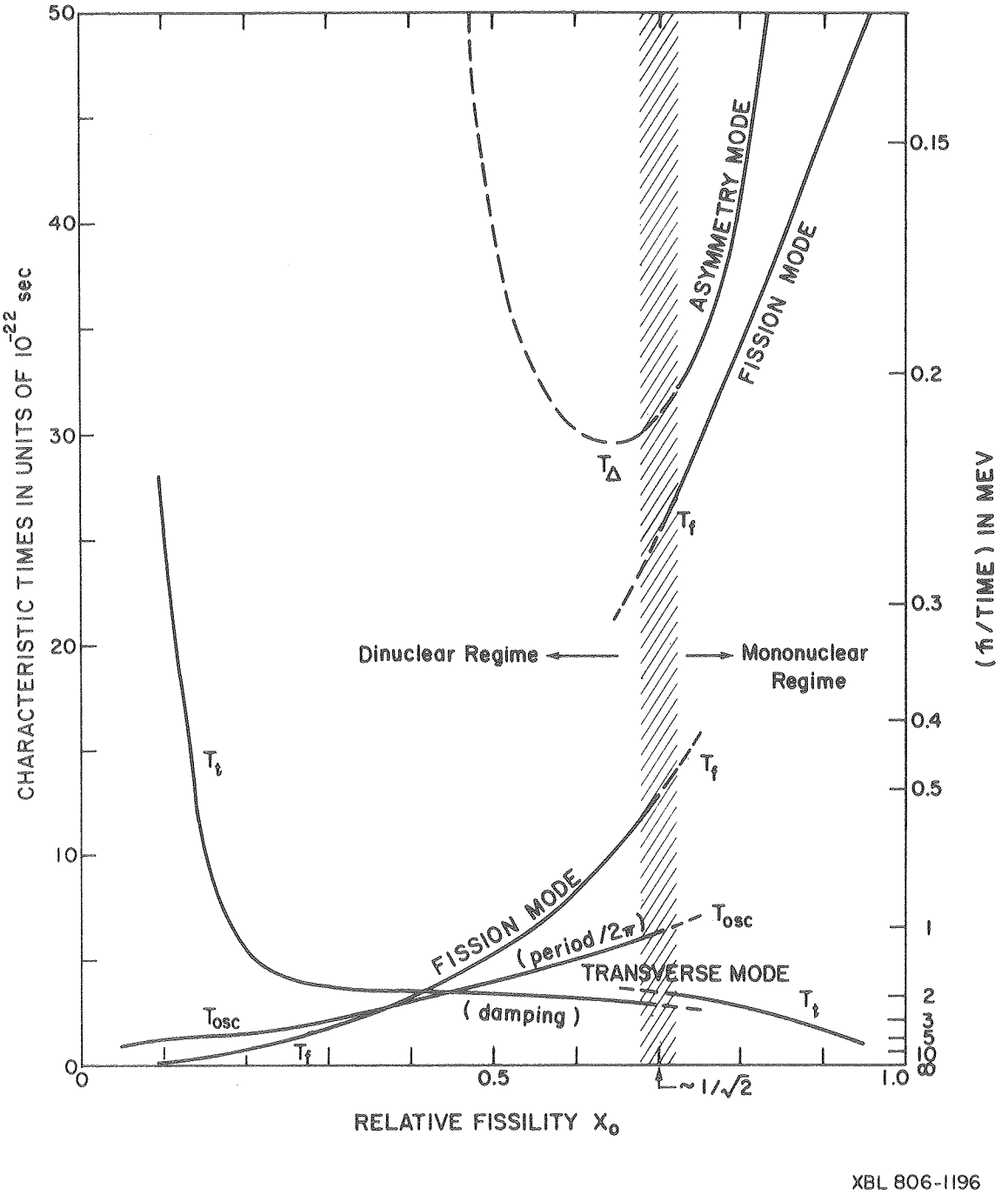

XBL 806-1196

Fig. 5

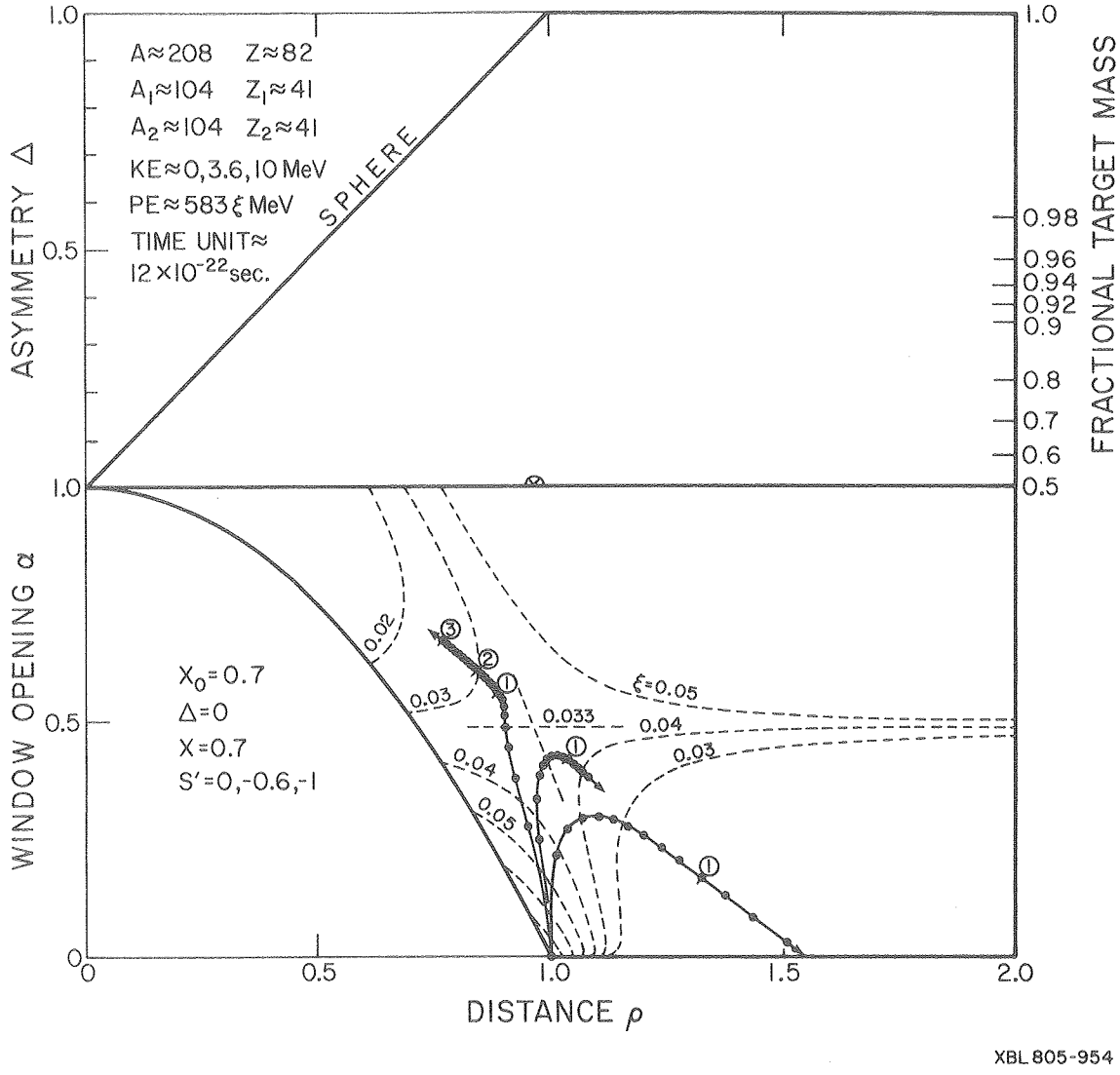

XBL 805-954

Fig. 6

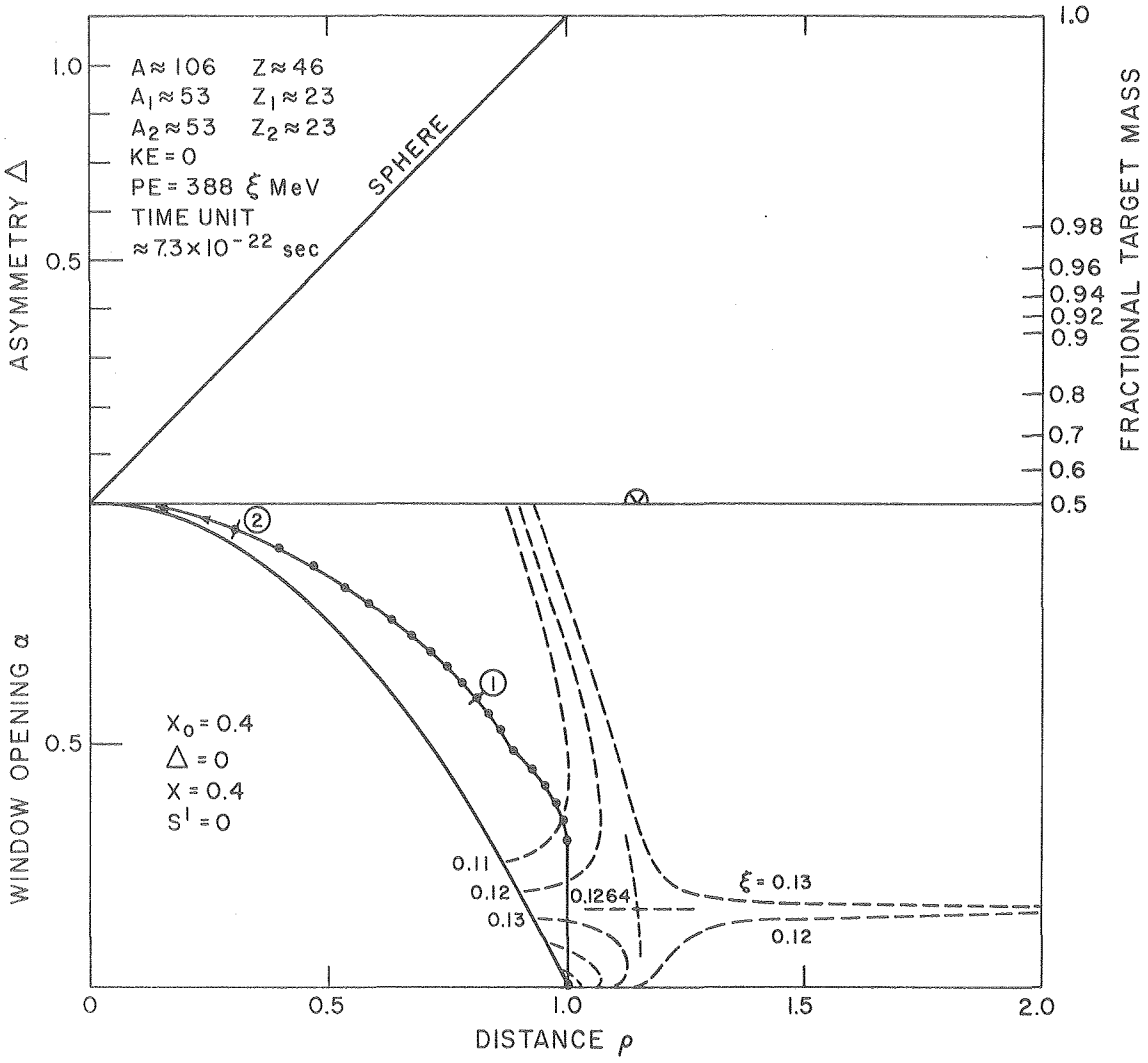

XBL 806-1202

Fig. 7

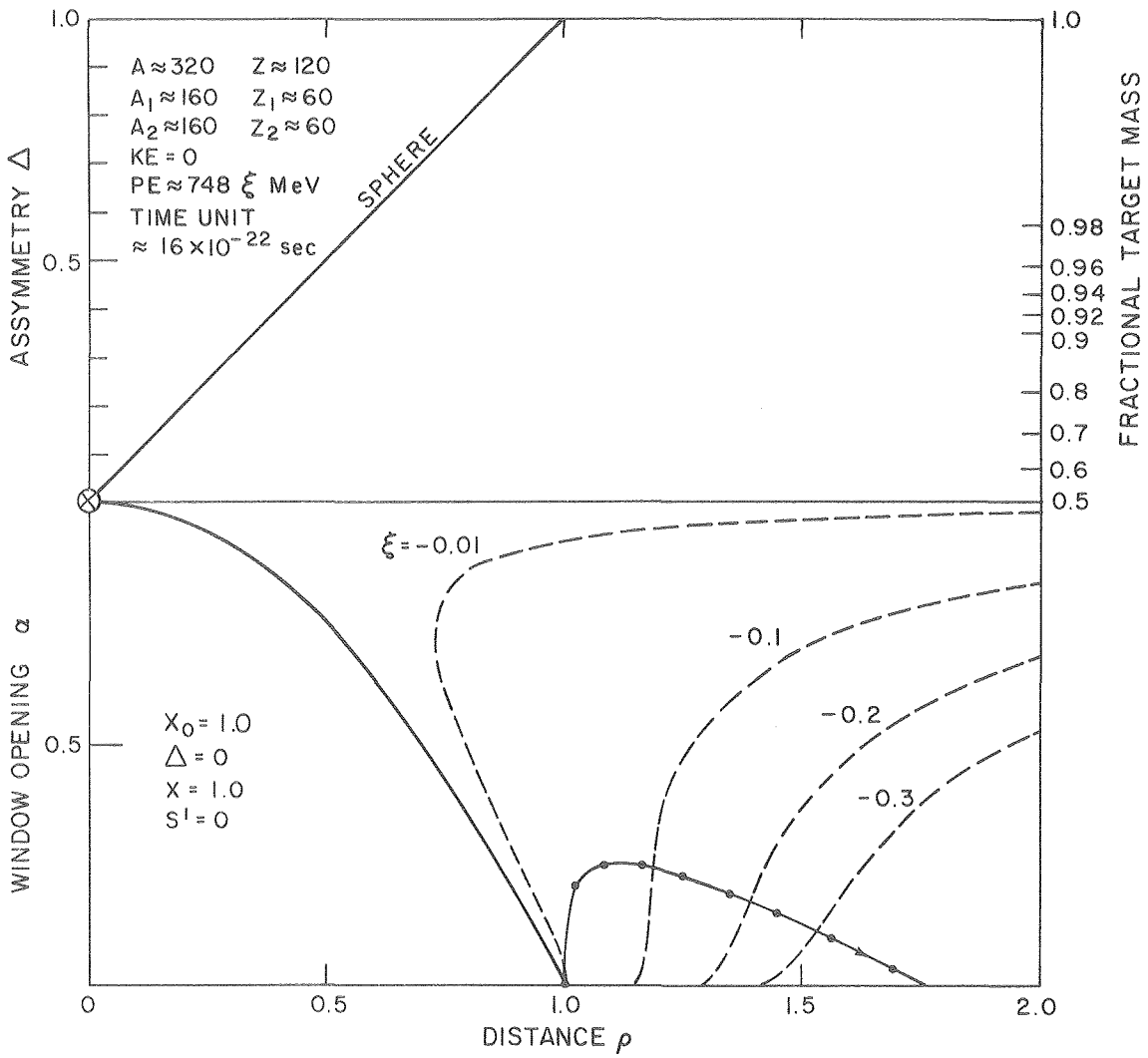

XBL 806-1203

Fig. 8

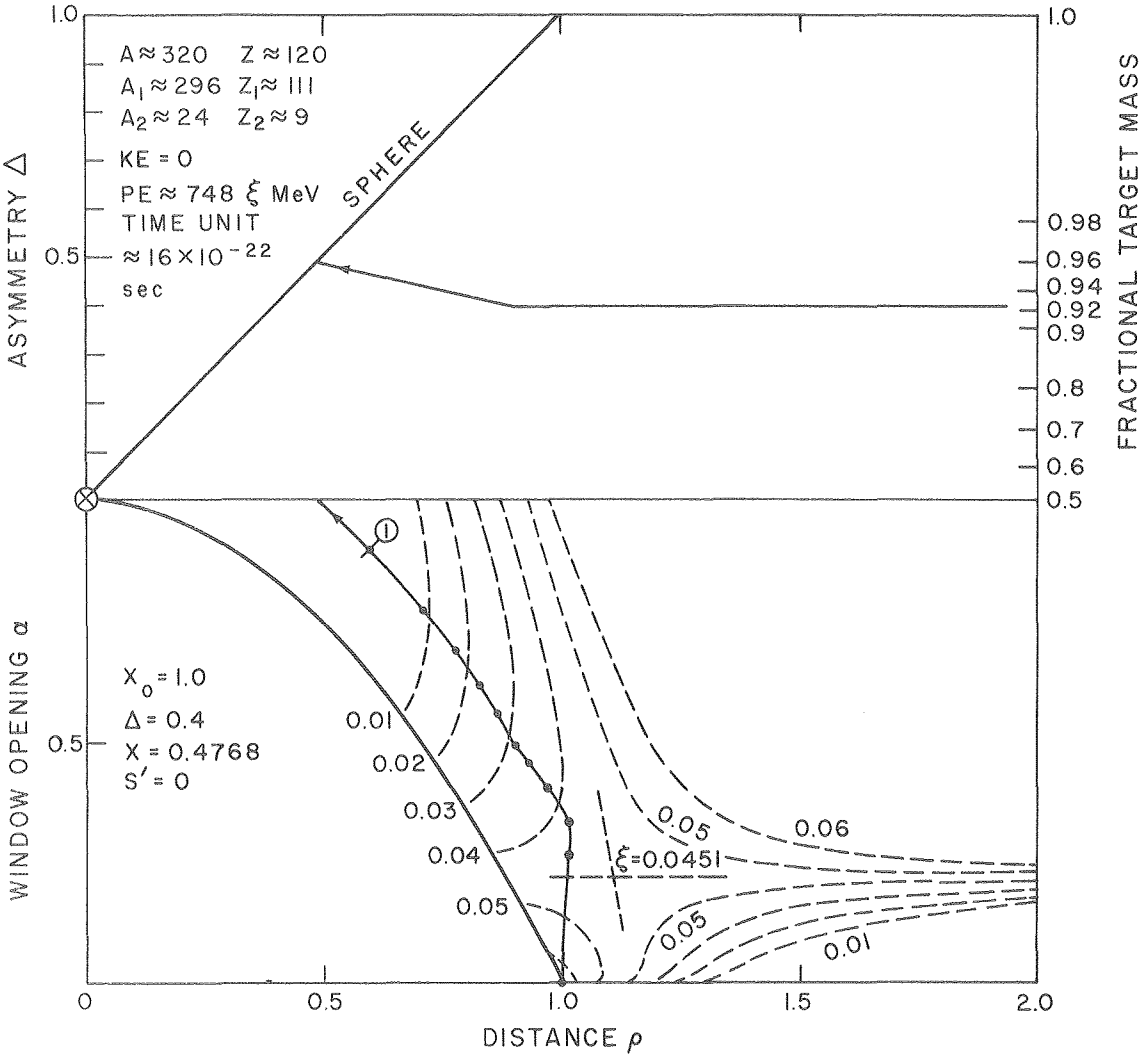

XBL 806-1199

Fig. 9

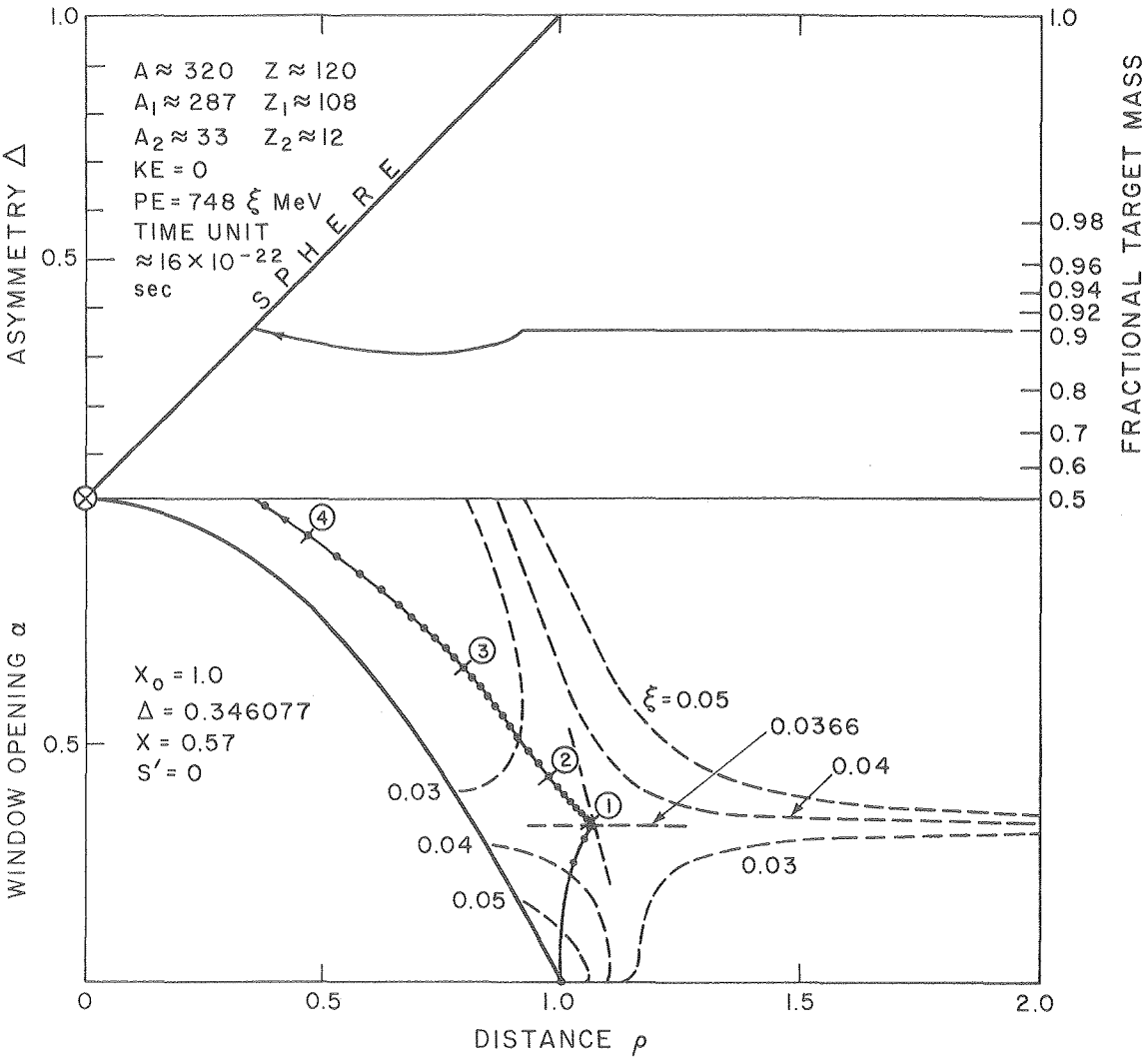

XBL 806-1197

Fig. 10

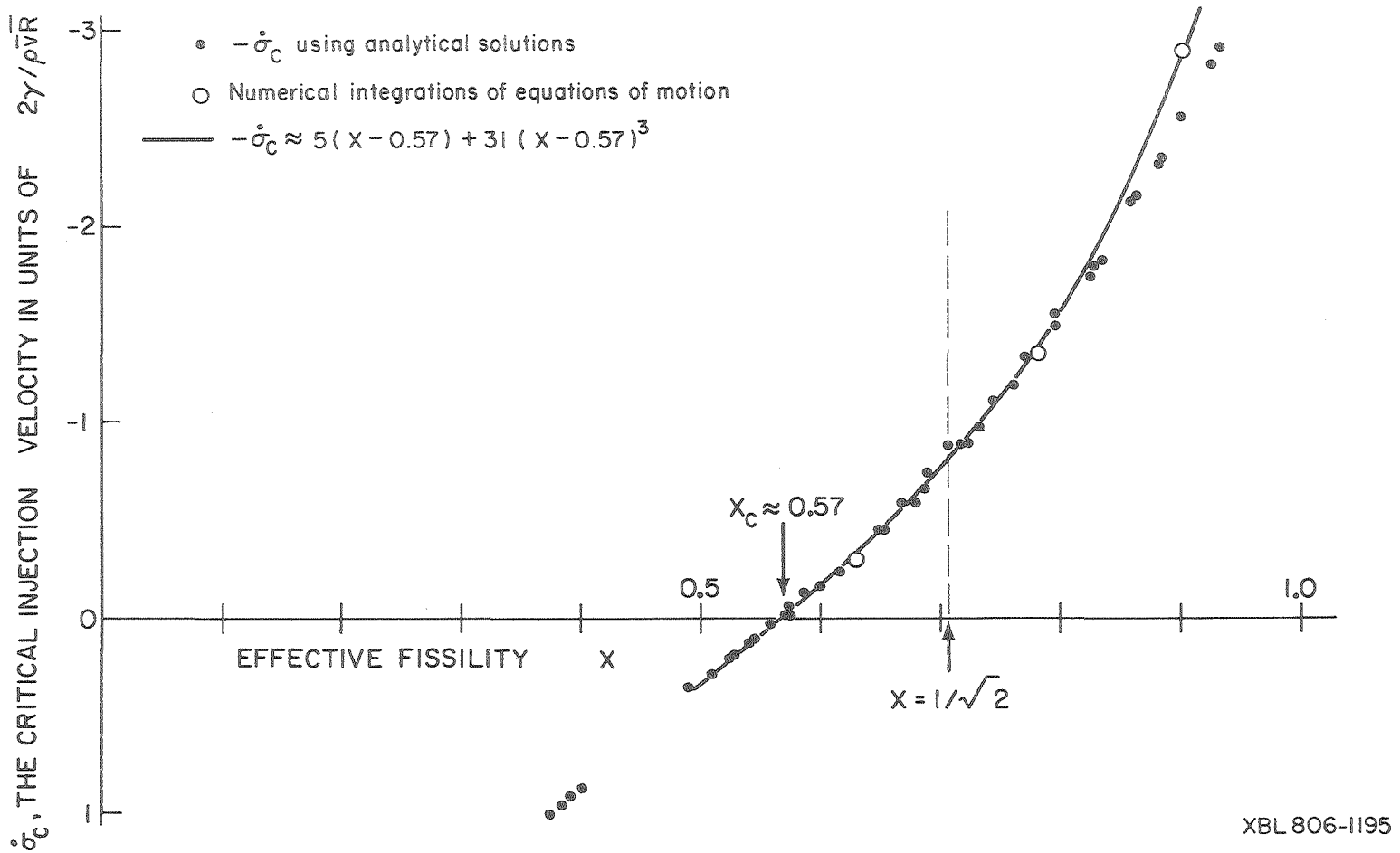
$\dot{\sigma}_c$, THE CRITICAL INJECTION VELOCITY IN UNITS OF $2\gamma/\rho\bar{v}\bar{R}$
-3
-2
-1
0
1
$-\dot{\sigma}_c$ using analytical solutions
Numerical integrations of equations of motion
$-\dot{\sigma}_c \approx 5(X-0.57)+31(X-0.57)^3$
$X_c \approx 0.57$
0.5
1.0
EFFECTIVE FISSILITY X
$X = 1/\sqrt{2}$
XBL 806-1195

Fig. 11

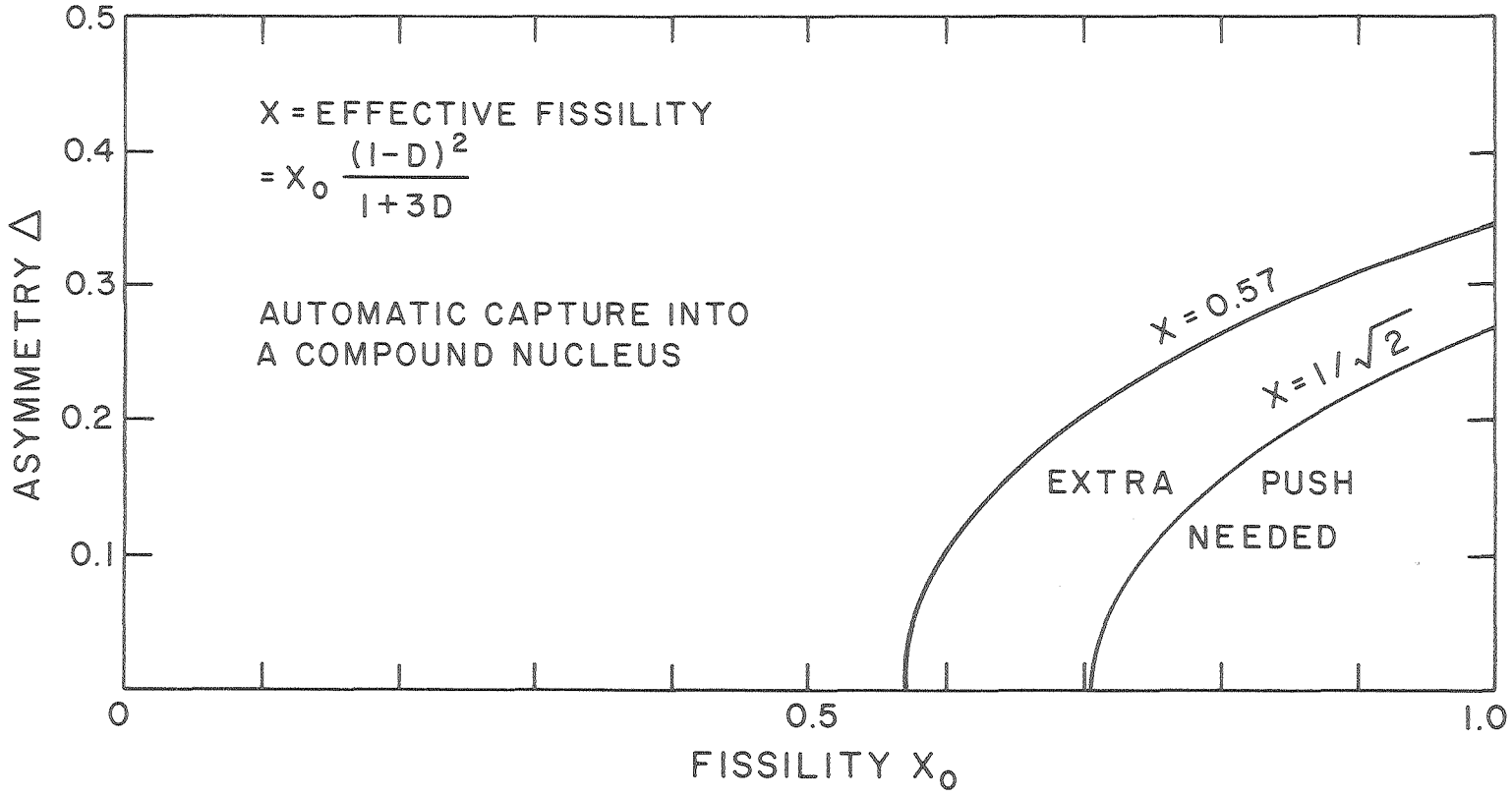

XBL 806-1204

Fig. 12

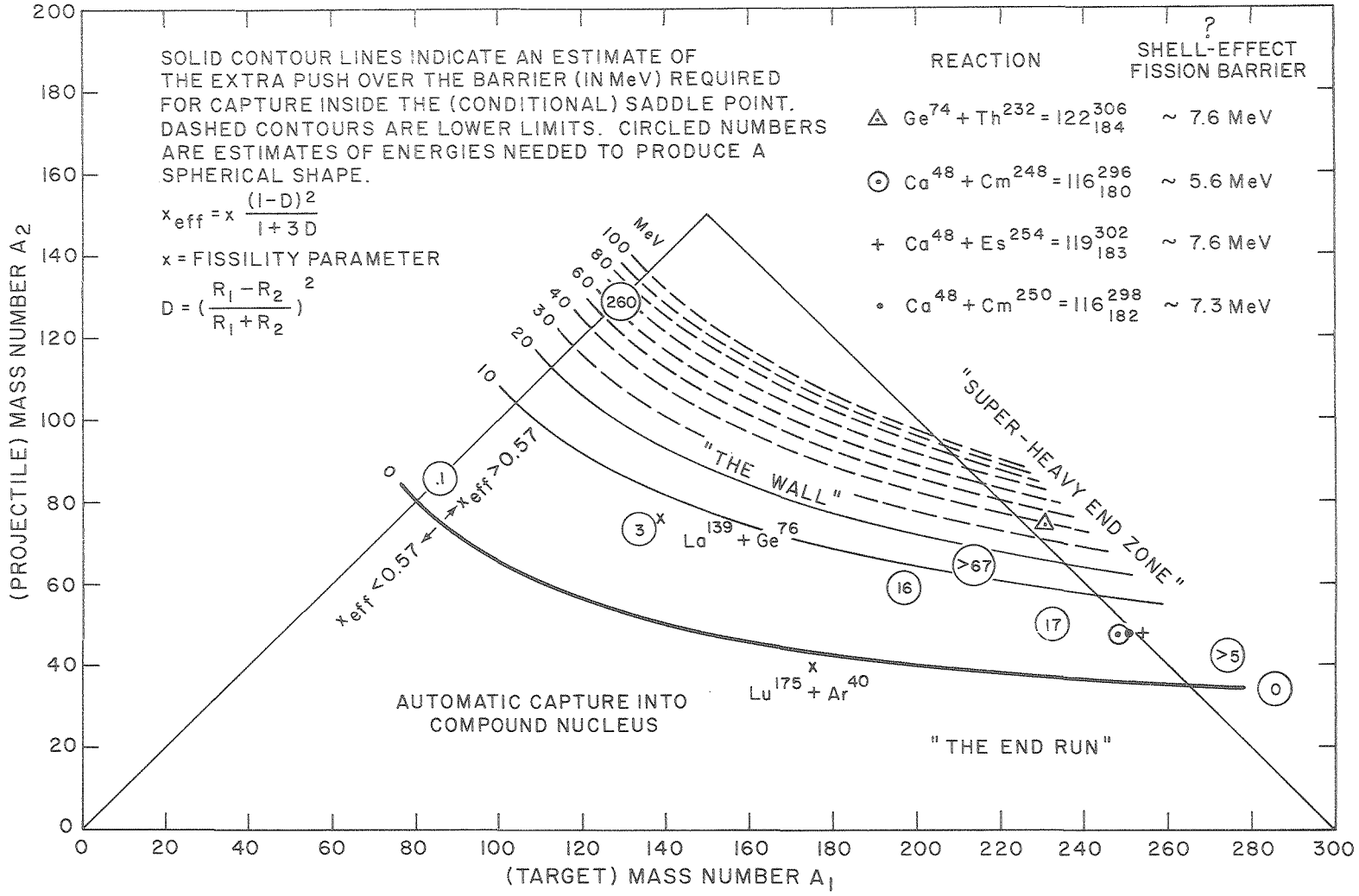

XBL 806-1201

Fig. 13

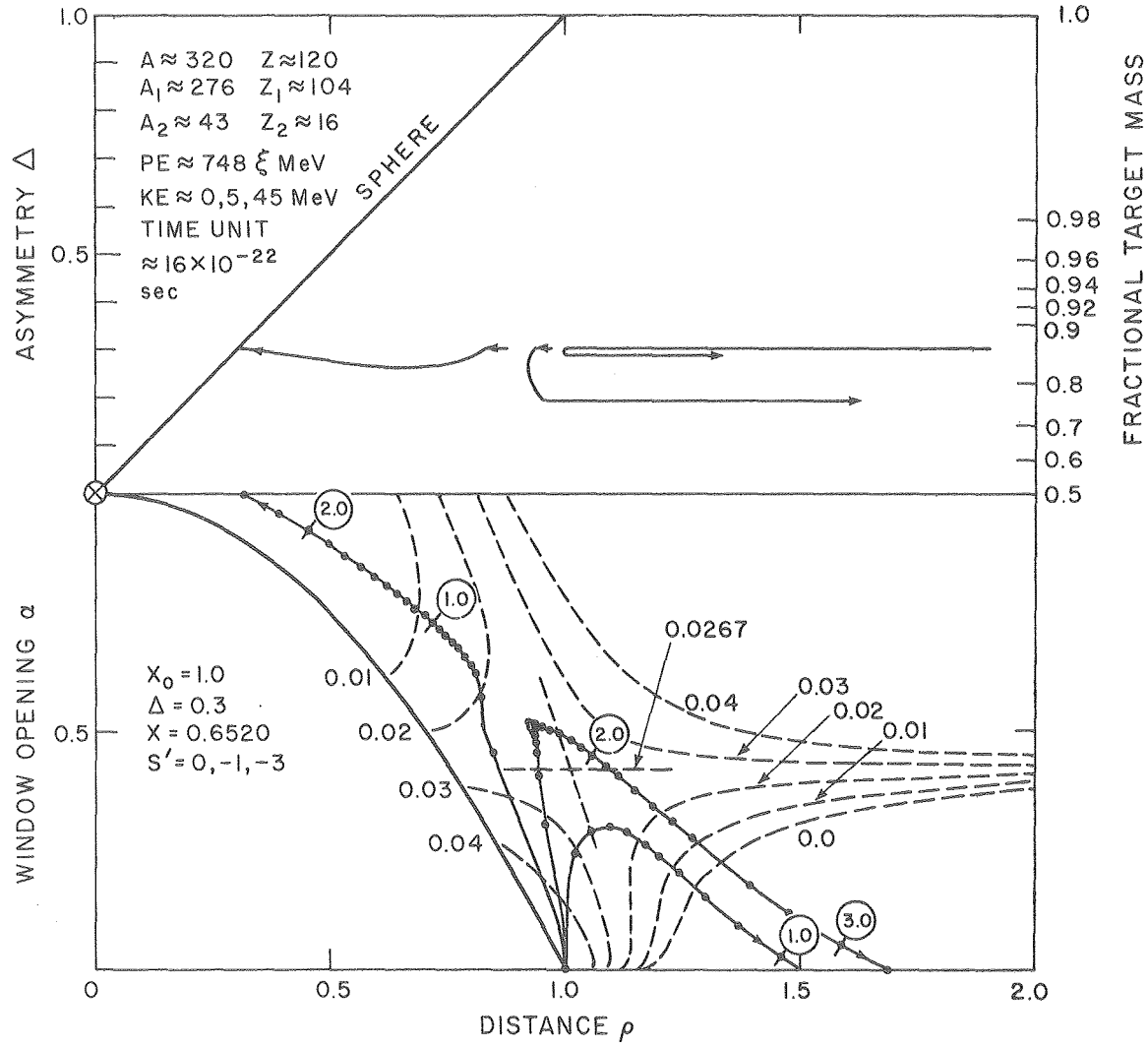

XBL 806-1198

Fig. 14

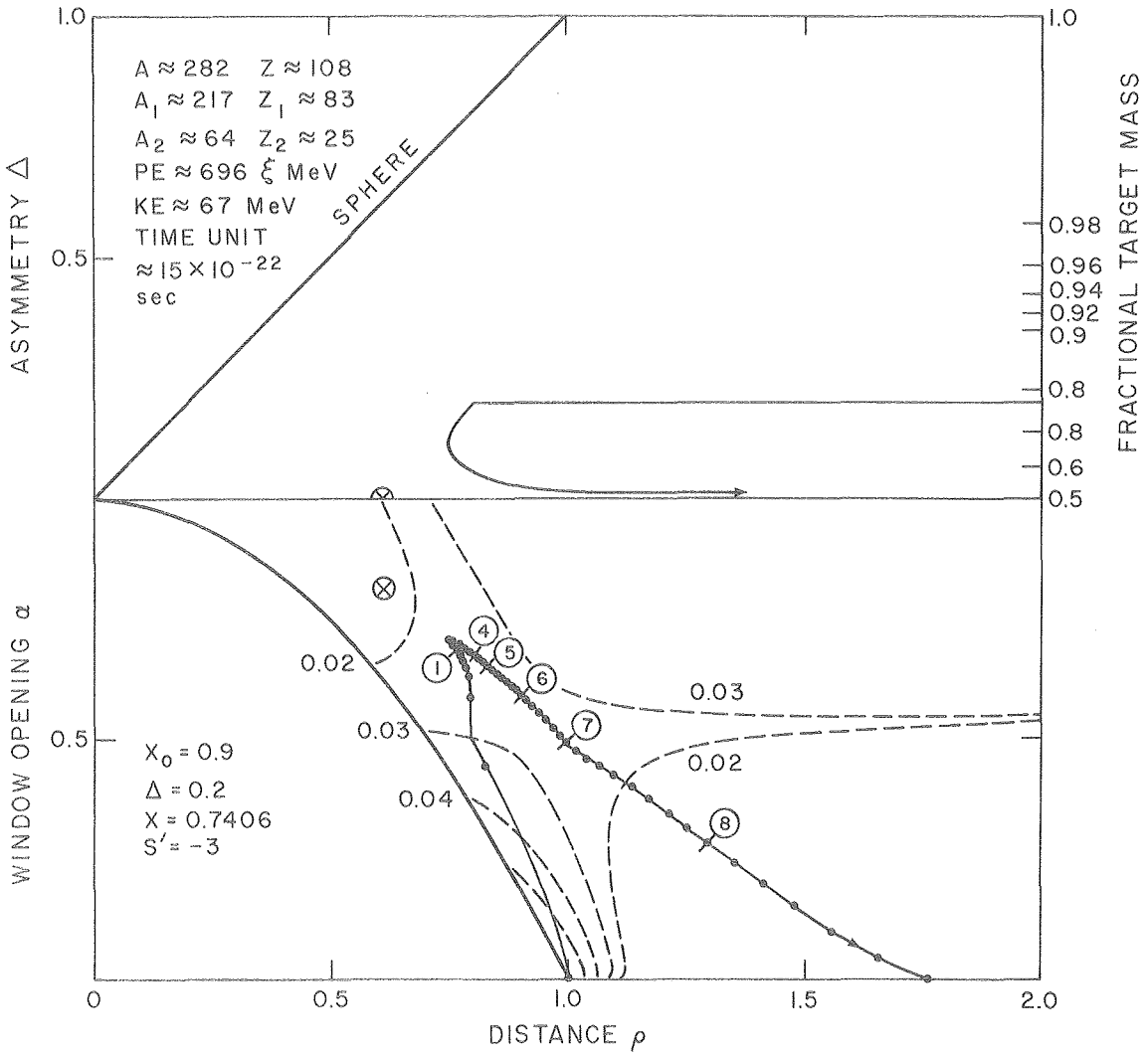

XBL 806-1200

Fig. 15

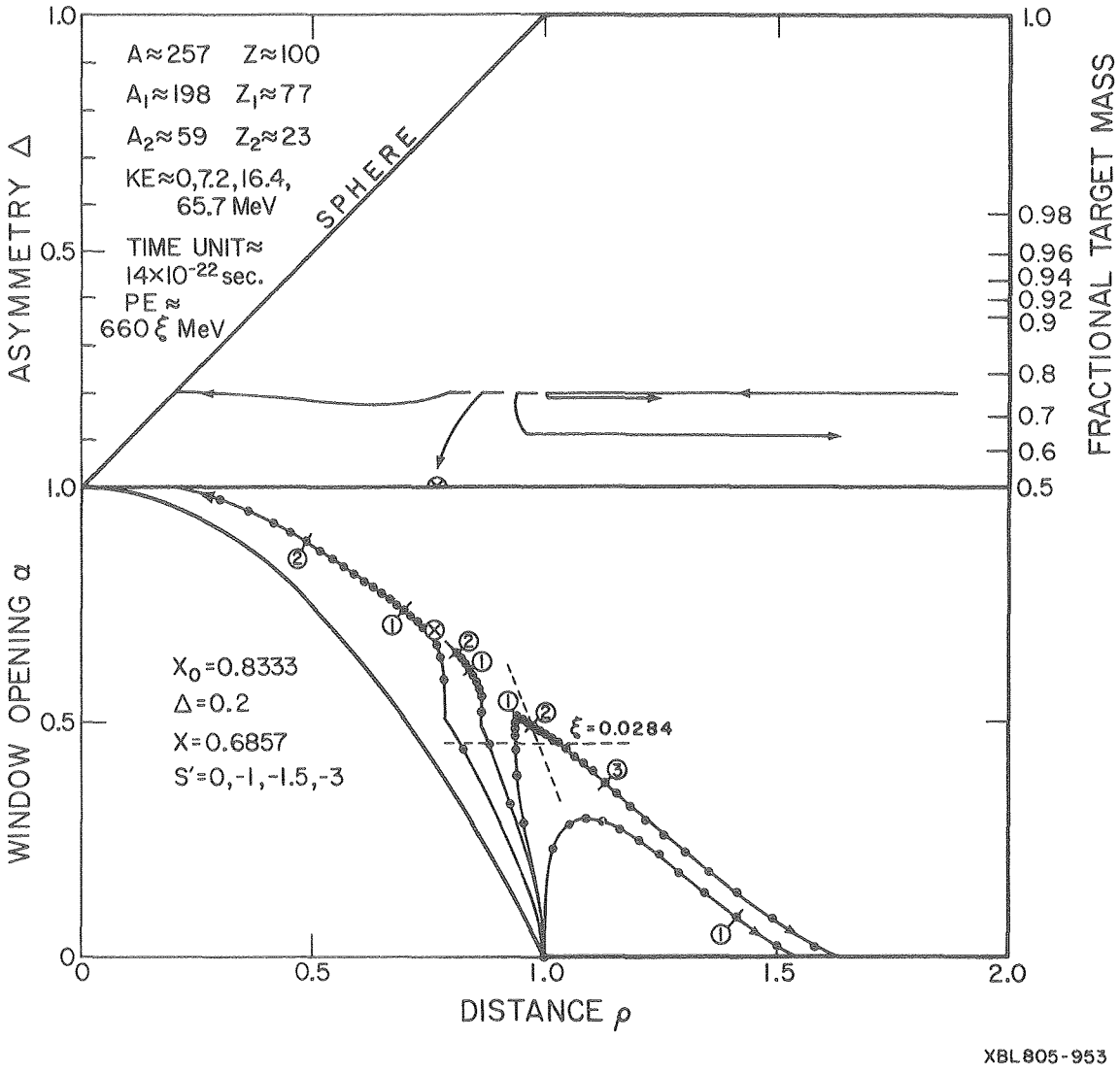
A≈257 Z≈100
A1≈198 Z1≈77
A2≈59 Z2≈23
KE≈0,7.2,16.4, 65.7 MeV
TIME UNIT≈ 14×10⁻²² sec.
PE ≈ 660 ξ MeV
SPHERE
ASYMMETRY Δ
WINDOW OPENING α
FRACTIONAL TARGET MASS
X0=0.8333
Δ=0.2
X=0.6857
S'=0,-1,-1.5,-3
ξ=0.0284
DISTANCE ρ
XBL805-953

Fig. 16

TECHNICAL INFORMATION DEPARTMENT
LAWRENCE BERKELEY LABORATORY
UNIVERSITY OF CALIFORNIA
BERKELEY, CALIFORNIA 94720